

COMPARING MODEL PREDICTIONS OF HILLSLOPE SEDIMENT SIZE
DISTRIBUTION WITH FIELD MEASUREMENTS

A thesis submitted to the faculty of
San Francisco State University
In partial fulfillment of
the requirements for
the Degree

MS
36
2018
GEOLOGY
M35

Master of Science

In

Geoscience

by

Mobin Mahmoudi

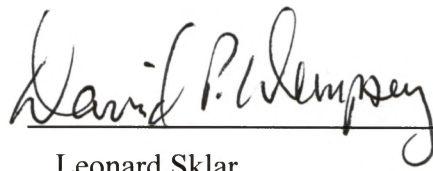
San Francisco, California

Spring 2018

Copyright by
Mobin Mahmoudi
2018

CERTIFICATION OF APPROVAL

I certify that I have read *COMPARING MODEL PREDICTIONS OF HILLSLOPE SEDIMENT SIZE WITH FIELD MEASUREMENTS* by Mobin Mahmoudi, and that in my opinion this work meets the criteria for approving a thesis submitted in partial fulfillment of the requirement for the degree Master of Science in Geoscience at San Francisco State University.


Leonard Sklar
Prof. of Geography, Planning
and Environment
Concordia University, Montreal, Canada

(Prof. of Meteorology
& Assoc. Prof. Chair
Dept. of Earth
Climate Sci.)
for Leonard
Sklar.


Jerry Davis
Professor of Geography & Environment
San Francisco State University


Alexander Stine
Asst. Professor of Earth & Climate Science
San Francisco State University

COMPARING MODEL PREDICTIONS OF HILLSLOPE SEDIMENT SIZE WITH
FIELD MEASUREMENTS

Mobin Mahmoudi
San Francisco, California
2018

Hillslopes produce the sediments that are supplied to river channels' bed. The river bed sediments link climatic factors to landscape evolution by regulating the rate of river incision. However, the factors that control hillslope sediment size are poorly understood, limiting our ability to predict sediment size and model the evolution of sediment size distributions across landscapes. Recently separate field and theoretical investigations have begun to address this knowledge gap. Here we compare the predictions of several emerging modeling approaches to landscapes where high quality field data are available. Our goals are to explore the sensitivity and applicability of the theoretical models in each field context, and ultimately to provide a foundation for incorporating hillslope sediment size into models of landscape evolution. The field data include published measurements of hillslope sediment size from the Kohala peninsula on the island of Hawaii and tributaries to the Feather River in the northern Sierra Nevada mountains of California, and the Inyo Creek catchment of the southern Sierra Nevada. These data are compared to predictions adapted from recently published modeling approaches that include elements of topography, geology, structure, climate and erosion rate. This research suggests that models may be suitable for predicting sediment size distribution, given adequate data for environmental factors and the initial size distribution is available.

I certify that the abstract is a correct representation of the content of this thesis.

David P. Dempsey (for Leonard Sklar)
Chair, Thesis Committee

5/21/18
Date

ACKNOWLEDGEMENTS

For assistance in data processing and writing, I first thank Shirin Leclere for her wonderful advice and insight into my project. For ideas, and far-ranging discussions, I thank my primary advisor, Leonard Sklar, my committee members Jerry Davis and Alexander Stine, as well as everyone in the both the Earth & Climate Sciences Department and the Department of Geography & Environment at SFSU. I thank my close friends Jack Reeder and Gionata Bianchi who helped me throughout the two years of earning my master's degree and helped me with the process of writing my thesis. They made sure that I was on track and constantly reminded me of important dates and deadlines. Finally, I would like to thank my wonderful family for supporting me financially in the course of my studies, and also helping me through any and all difficulties I encountered; especially my wonderful brother, Armin, who has been by my side at all times helping me with any difficulties I encountered.

TABLE OF CONTENTS

List of Tables	viii
List of Figures	ix
1 Introduction & Background	1
2 Predicting hillslope sediment size.....	2
2.1 Chemical Weathering Potential	3
2.2 Multiple Regression: Sediment Size Empirical Model.....	6
2.3 Fractal Model (Inyo Creek)	6
3 Study Sites	7
3.1.0 Inyo Creek.....	7
3.1.1 Geomorphology of Inyo Creek	8
3.1.2 Data collection at Inyo Creek	8
3.2.0 Feather River.....	9
3.2.1 Geomorphology of Feather River	9
3.2.2 Data collection at Feather River	9
3.3.0 Kohala Peninsula	10
3.3.1 Geomorphology of Kohala Peninsula.....	10
3.3.2 Data collection at Kohala Peninsula	11
4 Methods.....	11
4.1.0 GIS Maps	12
4.1.1 Slope Gradient, Aspect, and Solar Radiation.....	12
4.1.2 Temperature and Precipitation.....	13

4.2.0 Parameters for CWP and multiple regression models	13
4.2.1 Erosion Rate.....	14
4.2.2 Weathering.....	14
4.3.0 Regression.....	15
4.3.1 Normalizing attributes	15
4.3.2 Multiple Regression.....	16
4.4 Fractal Model.....	17
4.5 Size Distribution extrapolation	17
5 Results.....	18
5.1.0 CWP Predictive Model	19
5.1.1 Inyo Creek.....	19
5.1.2 Feather River.....	23
5.1.3 Kohala Peninsula	24
5.2.0 Multiple Regression Analysis.....	26
5.2.1 Inyo Creek.....	26
5.2.2 Feather River.....	27
5.2.3 Kohala Peninsula	28
5.3.0 Fractal Model.....	29
6 Discussion.....	31
6.1 Predictive Models	31
6.2 Future work.....	34
6.3 Landscape evolution Model Framework	35
7 Conclusion	37
References.....	39

LIST OF TABLES

Table	Page
1. Table 1.....	44
2. Table 2.....	44
3. Table 3.....	45
4. Table 4.....	45
5. Table 5.....	46
6. Table 6.....	47
7. Table 7.....	48
8. Table 8.....	48
9. Table 9.....	49
10. Table 10.....	49

LIST OF FIGURES

Figures	Page
1. Figure 1	50
2. Figure 2	51
3. Figure 3	52
4. Figure 4	53
5. Figure 5	54
6. Figure 6	55
7. Figure 7	56
8. Figure 8	57
9. Figure 9	58
10. Figure 10	59
11. Figure 11	60
12. Figure 12	61
13. Figure 13	62
14. Figure 14	63
15. Figure 15	64
16. Figure 16	65
17. Figure 17	66
18. Figure 18	67
19. Figure 19	68
20. Figure 20	69
21. Figure 21	70
22. Figure 22	71
23. Figure 23	72
24. Figure 24	73
25. Figure 25	74
26. Figure 26	75
27. Figure 27	76
28. Figure 28	77

1. Introduction & background

The size distributions of sediment produced on hillslopes and supplied to river channels influence a wide range of fluvial processes, from bedrock river incision to the creation of aquatic habitats. River bedrock incision is the main mechanism for valley evolution. The relationship between channel incision into bedrock and the sediments supplied by surrounding hillslopes is well established (Sklar & Dietrich., 2004). Given that sediments are stream's primary tool for river-bed abrasion, their size distribution and the amount supplied by hillslopes to channels influences the rate of bedrock incision and longitudinal profile development of the river. In order to accurately predict channel incision, we must understand the factors controlling sediment size distribution (SSD) supplied to the channel by the surrounding hillslopes. Currently these factors are poorly understood (Dietrich et al., 2003), limiting our ability to predict sediment size and model the evolution of their distributions across landscapes.

Recently, separate field and theoretical investigations have begun to address this knowledge gap. Here I will be comparing the predicting ability of several emerging modeling approaches (Sklar et al., 2016; Leclere, 2017; Roy et al., 2016) in landscapes where high quality field data are available. This is done to investigate if it is possible to predict SSD accurately and reliably in a wide range of landscapes. My goal is to explore the sensitivity and applicability of the theoretical models in each field context, and ultimately to provide a foundation for incorporating hillslope sediment size into models of landscape evolution.

The field data include published measurements of hillslope sediment sizes mostly from the dry side of Kohala peninsula on the island of Hawaii (Marshall & Sklar., 2012) and tributaries to the Feather River in the northern Sierra Nevada ranges of California (Attal et al., 2015), and an unpublished data set from the Inyo Creek catchment of the southern Sierra Nevada (Leclere, 2017; Genetti, 2017). These data are compared to

predictions adapted from recently published modeling approaches that include elements of topography, climatic factors, lithology, and geomorphic processes such as erosion rate and weathering. Predictive models for each site are built in ArcGIS using field condition datasets such as: digital elevation model (DEM) topography that is used as a source for (slope gradient, aspect, solar radiation), bedrock geology data is used for local (lithology, mineralogy), climate data is used for extraction of local and global (mean annual precipitation and temperature), and finally to estimate the local erosion rates. If the model derived simulated data are found to be statistically significant in relation to local sediment sizes, a successful prediction for the SSD can be devised into a computationally tractable method for incorporating spatial variation in production of hillslope SSD in landscape evolution models (figure 1).

2. Predicting hillslope sediment size

To predict the hillslope SSD, one has to understand what factors control the size and evolution of the sediments. These factors include the physical weathering rates, chemical weathering rates, and the initial size distribution (table 1). Differential heat stress, frost cracking, tree throw, and debris flow are some examples of physical weathering that can impact the SSD. These factors are hard to quantify and therefore are generalized for my study sites, since there are multiple physical weathering processes involved. Same can be said about chemical weathering, where multiply processes such as hydrolysis, hydration, and differential mineral weathering can produce disparity in size evolution between individual particles. However, I assume the difference between chemical weathering processes is uniformly applied is negligible. Therefore, here I mainly focus on the chemical weathering rates, which controls the sediment evolution. Also I will use bedrock fracture spacing, mineral crystal sizes, and some landslide data, depending on the study location and availability of data, to representation the initial size distribution.

2.1 Chemical Weathering Potential

The first model for predicting SSD is by quantifying the chemical weathering that affects the particles during their journey through soil, as proposed by Sklar et al., (2016).

Chemical weathering is controlled by water residence time, mineral solubility, climate factors such as temperature and precipitation, and the supply of fresh minerals to the surface by physical erosion. Thus, the potential for chemical weathering can be simplified to:

$$\text{Chemical Weathering Potential} = f(\text{Lithology, Climate, Tectonics})$$

Sklar et al. (2016) predicts the weathering of initial size distribution at a given location by quantifying the potential for chemical weathering, using the climatic factors of mean annual temperature and precipitation. Generally, the biotic factors are being controlled by climate and thus are assumed to be predicted by the climate parameter as well. Thus the chemical weathering potential (CWP) is defined as:

$$CWP = \left(\frac{P}{P_{max}}\right)^b e^{-\frac{E_a}{R}\left(\frac{1}{T} - \frac{1}{T_{max}}\right)} \quad (1)$$

where R = universal ideal gas constant, $b = 1/2$ and E_a is an activation energy the depends on rock type, T = temperature and P = precipitation. The constants (P_{max}) and (T_{max}) represent the global maximum for each variable and not for any given study region. The chemical weathering potential ranges from 0 for no chemical weathering to 1 for maximum chemical weathering. However, chemical weathering is also controlled by the amount of soluble minerals available. When all soluble minerals have completely weathered away, there is only insoluble minerals left. Even if climatic variables are at maximum force, the potential chemical weathering is still zero (Sklar et al., 2016).

However, the potential for weathering captured by CWP can only occur when the residence time for particles is long and the erosion rate is very low. As the particles spend a long time in the soil, the chemical reactions can reach equilibrium, and thus CWP is supply limited. Sklar et al. (2016) introduce a weathering function (W) which depends on CWP and the fraction of soluble minerals (F_{SM}), and express the supply-limited values of W as W_{SL} where:

$$W_{SL} = F_{SM} \cdot CWP \quad (2)$$

According to equation 2, W_{SL} is maximum when $F_{SM} = 1$ and no chemical weathering occurs when $F_{SM} = 0$. However, depending on the rate of erosion, three different scenarios of chemical weathering can occur. These scenarios are divided by two threshold values used in the following equation:

$$W = F_{SM} \cdot CWP \left[1 - \left(\frac{E - E_{SK}}{E_{KU} - E_{SK}} \right)^\varphi \right] \quad (3)$$

Here, E represents local erosion rate and the exponent φ is set to $2/3$ to capture the non-linear dependence of residence time of particles in soil. E_{SK} represents the threshold dividing supply-limited from kinetically limited weathering, and E_{KU} represents the threshold dividing kinetically limited chemical weathering from the case where fresh rock is supplied to the channel (i.e. no chemical weathering). When erosion rates are negligible, the chemical weathering processes have the most time to weather down the minerals and CWP is only limited by the supply of minerals ($E < E_{SK}$). But as erosion rates increase, and become larger than E_{SK} , ($E_{KU} > E > E_{SK}$), the particles spend less time in the soil and are less exposed to the chemical weathering processes; thus the CWP becomes kinetically limited. Finally, when erosion rates are high ($E > E_{KU}$), the residence time is low enough that the chemical weathering becomes negligible (figure 2). This is because the sediment residence time and its interaction with water (Burke et al., 2007;

Dixon et al., 2009; Riebe et al., 2001; Schmidt, 2009). The longer the mineral or rock particle is in contact with water, the higher the likelihood of chemical weathering, which yield finer SSD (Phillips et al., 2008).

After establishing the link between climatic factors and weathering Sklar et al., (2016) used the following transformation function to estimate the size distribution supplied to a given channel (D_C) based on measured initial size distribution (D_0):

$$D_C = D_{min}^W * D_0^{(1-w)} \quad D_{min} = 10^{-3}mm \quad (4)$$

where W ranges between 0 (no weathering) to 1 (complete weathering). D_{min} represents the minimum particle size that would be considered bedload. Here, I mainly focus on particle sizes above 10^{-3} mm, as anything below that can be considered dissolved load. River incision require saltating bedload, and dissolved load has negligible impact on bedrock incision, unless the bedrock is dominated by soluble rocks such as carbonates, which our study locations lack. Sklar et al. (2016) assumes that chemical weathering only has an impact on hillslopes, while physical weathering only affects the initial size distribution governed by initial bedrock conditions, such as bedrock spacing which determines the maximum initial sizes that are possible (figure 3).

Using the transformation function (eqn. 4) for varying CWP fractions, I was able to produce a range of SSDs supplied to the channel, as shown on figure 4. After applying this equation to each size class in the distribution, the mass fraction in each size class gets transformed to the new sizes. Depending on the strength of CWP, the new sizes should have smaller mean and median. In theory, the size distribution observed in the field, compared to the initial size distribution data, should follow a straight line in the power function plot similar to figure 4. However, as will be discussed later in the results section, this was not always the case.

2.2 Multiple Regression: Sediment Size Empirical Model

A second approach to predicting hillslope sediment size is to use field data to build an empirical prediction relationship using multiple regression. This is done by constructing a log-linear or power law best fit model for predicting the median SSD (D_{50}) for a given study location. This fitting equation can be expressed as a log-linear plot:

$$\text{Log}_{10}(D_{50}) = \text{intercept} + aX_1 + bX_2 + cX_3 + \dots + nX_n \quad (5)$$

or can be expressed as power function:

$$D_{50} = K * X_1^a * X_2^b * X_3^c * \dots * X_n^n \quad K = 10^{\text{intercept}} \quad (6)$$

Here, the symbols (X_1, X_2, \dots, X_n) represent different topographical or climatic variables and lower case letters (a, b, c, \dots, n) represent the variable's statistical coefficients derived from the multiple regression solution. Thus if local topographical and climatic variables are known, using these equations, local D_{50} can be predicted. While this empirical fit model only represents the central tendency, the median, of the size distributions, it is possible to use the same fit model for quantiles other than D_{50} . Previous studies in each location point toward different variables as the main control in SSD. So by producing an empirical fit model, I can test previous findings and see if there is any additional statistical support for those claims.

2.3 Fractal Size Distribution Model

The third model used here is the fractal model. What sets the fractal model apart from the other two methods is that, it is used to predict the initial size distribution rather than the size distribution that is supplied to the channel. I use bedrock fracture spacing as a possible control on initial size distribution and assume this relationship follows a linear power law function (Roy et al., 2016). If the bedrock fracture spacing has a fractal

distribution, then the fractal model should be able to predict initial SSD. The cumulative fractal distribution can be written as:

$$N(>D) \geq kD^{-D_F} \quad (7)$$

where N is the number of particles; D is the diameter of particles, D_F is the fractal dimension and K is a pre-factor which represents the value of N when D = 1mm. Using this model, it should be possible to predict a full range of the initial sizes distribution using a small sub-sample. This relationship has been used in models investigated by Egholm et al., 2013 and Roy et al., 2016. This is very useful for extrapolating data for a large region using few samples.

3. Study Locations

I focus on three regions: two located in the Sierra Nevada Mountains of California, and one on in the Kohala Peninsula of the big island of Hawaii. I chose the locations because of previous research where enough data was available for me to be able to conduct my research. I chose the Kohala peninsula particularly because of the difference in lithology compared with the other two sites; where all California sites are composed of mainly granodiorite while Hawaii is made up of mainly basalt. This way I could investigate the impact of varying rock rigidity as one of the controls on evolution of SSD.

3.1.0 Inyo Creek

The first study site is located just southeast of Mt. Whitney on the east facing side of the southern Sierra Nevada mountains (figure 5). Inyo Creek is a relatively small watershed with surface area of 3.2 Km^2 , but fairly steep relief of little more than 2 km. This particular site was selected by number of previous studies (Riebe et al., 2015; Sklar et al., 2016; Stock et al., 2006; Hirt, 2007), and thus there is detailed data available on SSD and

the lithology of this watershed. The creek begins in the steep bedrock cliffs of the highlands and ends in piedmont leaving behind channeled alluvium.

3.1.1 Geomorphology of Inyo Creek

Inyo Creek has a dry climate, as it is located on the rain shadow side of the southern Sierra Nevada. As a result, even with the high relief of the Inyo Creek the precipitation difference throughout the span of the creek is not very different, ranging from 473 to 326 mm annually. Inyo Creek's bedrock is entirely made up of plutonic granodiorite, formed sometimes between 88 to 83 Ma (Hirt, 2007). The rigidity of the bedrock throughout the catchment is consistent enough to assume uniform lithology for predicting the SSD. The ridges surrounding Inyo Creek are steep. Unlike the Mount Whitney watershed located just to the north, there is no evidence for past glaciation in Inyo Creek (Stock et al., 2006).

3.1.2 Data collection at Inyo Creek

The data for Inyo Creek were taken from the work of Jennifer Genetti and Shirin Leclere for their Master's theses (figure 6). The findings from their work are part of the Sklar et al., 2016 paper which proposes a method for predicting SSD supplied from hillslopes to channels. The data sites were randomly selected within the watershed, specifically areas that were accessible, not in the creek, or near the ridges. The data samples are combination of point count measurements and bulk sampling. Ultimately, 19 locations were selected, but one location had to be discarded as it was too close to the creek. The location ranges in elevation from 2212 to 2875 m and range in slope from 23.8 to 47.3 degrees.

3.2.0 Feather River

The second study site is mostly within the watershed boundaries of Bald Rock Creek, one of the Feather River's tributaries. The Bald Rock Creek watershed is about 10 km east of Lake Oroville at the middle fork of the Feather River (figure 7). However, the sampling is not limited only to the Bald Rock Creek watershed. There are 3 point-count measurement available at a landslide outcrop nearby. These point counts were collected to investigate a possible initial size distribution and source of coarse sediment supplied to the river. This location was chosen because it was part of the Attal et al., 2015 study and thus there is comprehensive SSD data available online for me to use in this research.

3.2.1 Geomorphology of Feather River

This region of Feather River is moister and more vegetated than Inyo creek. Feather is also much less elevated than Inyo Creek and due to the small relief of our study sites, the temperature and precipitation difference between the sites are small. However, overall the geomorphic processes that control SSD should be very similar. Feather River is located in the northern parts of Sierra Nevada and this region is dominated with metamorphic basements. However, Bald Rock Creek is mostly composed of Mesozoic plutonic intrusion of granodiorite and tonalite over the metamorphic basement (Attal et al., 2015). Therefore, rock rigidity at this location should be similar to the granodiorite at Inyo Creek.

3.2.2 Data collection at Feather River

The data for Feather River was taken from supplementary materials available online as part of Attal et al., 2015 paper (figure 8). The data for this site was collected in two regions. One on the landslide outcrop region and other within the watershed boundary of Bald Rock Creek. The 9 sites within the watershed were selected based on their morphological differences. Three morphological regions were identified as bases for

sampling location, including: relict topography above the break in slope (POMD), in the transition zone where the hillslopes have not completely adjusted to the base-level fall (FTA), and below the break in slope (BRC and BRB) (figure 9). The landslide samples were taken from 3 different locations on the talus using a point count measurement. The location ranges in elevation from 637 to 787m and range in slope from 12.2 to 46.9 degrees.

3.3.0 Kohala Peninsula

The final study site is located on the Kohala Peninsula in big island of Hawaii. The sites were not chosen within any particular watershed. Most of the sites are on the south facing slope of the mountain, while one site is on the north facing slope (Figure 10). Although, this location was also chosen because of available data, the climate variation between the two sides of the peninsula made this location unique for studying the effects of climate on sediment evolution. Unfortunately, the SSD data for this location was limited to only 7 sites. Also, there are no point counts of fracture spacing, or mineral crystal, or landslide particles sizes for me to use as a reference for initial size distribution.

3.3.1 Geomorphology of Kohala Peninsula

Kohala Peninsula is very interesting to study due to a significant climatic differences between the two sides of the Peninsula, divided by a mountain ridge. Prevailing winds coming from Northeast, brings moisture to the North facing side of the Kohala. As a result, the north facing side is covered with lush rainforest and the south facing side is basically a desert. Lithology of the region is entirely made out of extrusive igneous basalt left behind from geologically recent (0.7Ma) volcanic eruptions (Wolfe & Morris, 1996), which distinguishes Kohala from the other two study locations.

3.3.2 Data collection at Kohala Peninsula

Much like the other locations, Kohala was chosen because of previous studies at this location (Marshall & Sklar, 2012) (Chadwick et al., 2003). The data used for Hawaii originates from the 7 pedons selected in Kohala as part of Marshall and Sklar, 2012 study on data mining for sediment size distribution. Pedons are 1 m^2 in surface area of soil pit that contains all soil horizons all the way to regolith. By averaging all horizons' distribution, I was able to produce a unified SSD for each of the 7 sites (figure 11). For my research I only needed the averages of the horizons to be consistent with other study locations. However, the lithology of this region makes it difficult to collection data that represents local initial size distribution. Hawaii is dominated by extrusive igneous basalt, with varying consistency and age. The extrusive nature of the rock would produce very different bedrock, one that has different fracture pattern than intrusive rocks of Sierra Nevada and it would have tiny mineral crystals embedded in the rock. The consistency of the bedrock can also vary widely from place to place due to chaotic nature of volcanic eruptions.

4. Methods

In order to test predictions of hillslope SSD, there are number of variables that needs to be considered. Before any analysis can be made, measurements of the size distribution need to be collected from a number of locations along a hillslope transect, for example from the ridge to the valley bottom. However, collecting this data is a significant operation as numerous pits need to be dug or many point counts need to be taken in difficult topographical settings. I decided to use existing data from previous studies for locations where the size distribution would meet the minimum requirements for my predictive models. These requirements include sediments size distribution samples with exact coordinates, available climate data (needed for calculating chemical weathering potential estimates), available lithological data, and fine resolution digital elevation

model (DEM) needed for producing a raster map of slope gradient, aspect, and solar radiation.

4.1.0 GIS Maps

Much of the spatial data needed for calculating CWP and the empirical fit models were produced using GIS raster maps. I first isolated the regions where the field measurement sites are located using the coordinates available from previous research and created attribute maps for those sites. These maps included: slope gradient, aspect, solar radiation, average annual precipitation, and average annual temperature. Using these rasters maps, I was able to extract point measurement associated with each specific site and finally construct a table with all the attributes necessary for sediment size prediction models.

4.1.1 Slope Gradient, Aspect and Solar Radiation

I downloaded 10 m resolution DEM rasters from the United States Geological Survey (USGS) for each of my study locations. Using standard ArcGIS Spatial Analyst functions, I was able to derive surface attributes such as slope gradient, aspect, and the net solar radiation received for each individual site. I chose these particular attributes because previous studies have suggested that slope and aspect are significant topographical controls on SSD (Langston et al., 2015; Leclere, 2017; Olyphant et al., 2016) (figure 12); where coarser grains are more associated with steeper gradients and low solar radiation, (north facing aspect) and finer grains are more associated with gentle gradient and high solar radiation (south facing aspect). However, using raw aspect alone would not give the most accurate representation of solar influence on weathering and the resulting SSD. The solar insolation doesn't necessarily peak when aspect is in one of the cardinal directions (N, S, E, W) and therefore the aspect needs to be normalized to better represent the effect solar radiation. I decided to use an ordination technique proposed by

Leclere, 2017 for normalizing the aspect in such a way that it is most correlated to net solar radiation.

4.1.2 Temperature and Precipitation

For the CWP (equation 1) and weathering (equation 3) part of the transformation function (equation 4), I needed mean annual temperature and precipitation, as well as global maximum values for each. For Kohala peninsula, I was able to use 100 m resolution raster data provided from Hawaii's official state website (Hawaii.gov) that was accurate enough for me to be able to get detailed temperature and precipitation estimates for each of the 7 sites. However, for Inyo Creek and Feather River, there was no local data available and I only able use free data available from University of Oregon Climate Group PRISM (PRISM, 2016). PRISM is a large spatial scale climatic estimate, with 4km spatial resolution. Each individual pixel was larger than the entirety of my study sites in California. For Inyo Creek, this data was extrapolated based on two pixels that encompassed the watershed at 2000 m and 4000 m elevations. However, for Feather River individual sites were clustered in two separate locations, cluster one (POMD sites) and cluster two (BRC and FTA sites). Each cluster was located in a different pixel with 4 km resolution, therefore I just used the values for the individual pixels. There was no need to extrapolate the data because the sites are within 100 meters of each other. The mean annual temperature variation used for Inyo Creek, Feather River, and Kohala Peninsula are: (-1 to 10 °C, 14.2 to 15.4 °C, 12.9 to 19.2 °C) respectively. The mean annual precipitation variations are: (325.7 to 472.5 mm, 1567.5 to 1576.4 mm, 226.9 to 3193.6 mm) respectively (tables 2 to 4).

4.2.0 Parameters for CWP and multiple regression models

In order to come up with an accurate empirical model for predictive SSD, I wanted to consider as many attributes as possible while doing the multiple regression analysis. I had

access to aspect, solar radiation, precipitation, temperature, elevation, and D_{50} . However, aspect and solar radiation are correlated with another and precipitation and temperature are proxies of elevation in all locations, as elevation is the main determining factor for those attributes. So I needed a different attribute to focus on and weathering is most likely the main control on the evolution of sediments. Therefore, I decide to calculate erosion rates and weathering for all the sites to use in my multiple regression model. Using Sklar et al. 2016 equations combined with GIS data available for topographic and climatic attributes, it is now possible to estimate site specific erosion rate and weathering.

4.2.1 Erosion Rate

One of the most important factors controlling the supply of sediment is the erosion rate. By quantifying the erosion rate, one can estimate the SSD available for the weathering process to be applied to. Here, the erosion rate is dependent on elevation as a best-fit exponential equation, established by Riebe et al. (2015) as part of their Inyo Creek study. This equation is written as:

$$E = 0.22e^{2\left(\frac{Z-Z_{max}}{\Delta Z}\right)} \quad (8)$$

where Z represents the elevation in meters above sea level, Z_{max} the maximum elevation, and ΔZ as maximum change in elevation for all the sites. With erosion rate now calculated, I was able to calculate weathering for each site.

4.2.2 Weathering

To calculate weathering using the erosion rates, the equation (3) was used. I needed to parameterize the values for precipitation, temperature, and number of other constants for each specific site. For CWP the following values were used: $R = 8.3$ J/Kmol for the universal ideal gas constant, exponent $b = 0.5$, and the activation energy E_a was given a value of 60 kJ/mol for granitic rock in the Sierra (Riebe 2004; West et al., 2005), or 42

kJ/mol for Kohala Peninsula (Chadwick, 2003). The temperature and precipitation values are extrapolated from PRISM data as mentioned before, where the resolution of the raster was not high enough to make individual measurements for each site. The temperature and precipitation are dependent on elevation for Feather River and Inyo Creek. However, for Kohala Peninsula there was a much more detailed, high resolution raster, available from the State Government's website which I used as a source.

4.3.0 Regression

For the second model, I constructed a predictive model for SSD based on statistical analysis of different attributes and tested those attributes for their level of statistical significance. After which, I derived a number of empirical fits, for each of the study sites, using the most significant topographical and climatic attributes. This was done to predict the median sediment size (D_{50}) tailored for each of the study sites. Depending on the sediment size of interest, i.e. ($D_{30}, D_{50}, D_{84}, etc \dots$) this predictive model can be adjusted to predict a particular size. However, I was only interested in D_{50} here, so I only focused on that. All the statistical analysis carried out in this research was done using JMP statistical analysis software.

4.3.1 Normalizing attributes

Before constructing the fit models, I normalize all of my attributes to eliminate the units of measurement and unit conversion problems for my data. This process enables me to be able to easily compare data from different attributes and be consistent in doing the regression analysis. I used two common methods of normalizing data: 0.05 to 0.95 range normalization which is a modified version of 0 to 1 range normalization, and the Z-score method of normalization. The first method is as follows:

$$Attribute_{norm} = 0.05 + \frac{0.9*(x - x_{min})}{x_{max} - x_{min}} \quad (9)$$

The reason for choosing 0.05 to 0.95 range is to be as close to 0 to 1, without using 0 as the minimum value. I log transform my data for empirical best-fit models, therefore the presence of 0 would cause mathematical problems as log function approaches negative infinity while closing on zero, and thus is not defined. The second method for normalization was the standard z-score, which is as follows:

$$Z_{score} = \frac{x-\mu}{\sigma} \quad (10)$$

Here, μ represents the mean and σ represents the standard deviation for the sample data set. I needed to produce Z_{score} normalized data sets to be able to compare and contrast my attributes and run z-test, while investigating the best predictive empirical fit model.

The normalization discussed previously were applied to slope gradient, precipitation, temperature, erosion, and weathering. However, the effect of aspect on SSD does not vary linearly. That is because it is dependent on the net solar radiation received at each individual location. Therefore, I decided to rotate the aspect for each site based on the best correlation of aspect to solar radiation I could get testing all angles from 10 to 360 degrees. After determining the most appropriate rotation, the aspects were rotated using the following equation:

$$Aspect_{norm} = \frac{\cos(x-r)+1}{2} \quad (11)$$

where x is the local aspect in degrees and r is the rotation reflecting the strongest solar insolation effect.

4.3.2 Multiple Regression

The primary purpose for running a multiple regression analysis is to find which attributes correlate most closely to output D_{50} and construct an empirical formula for predicting D_{50} based on any location's attributes. Here, I first tested the correlation of every single

attribute to D_{50} and built a R-squared and statistical coefficient data set which is needed for the empirical fit model. After which, by the process of elimination, I isolated the top three most correlated attributes as the main candidates for explaining variables. I also recorded the y-intercept for the multiple regression fit of the top three attributes. Using all these values extracted from JMP, I was able to produce three different empirical fit equations for three different study locations I had.

4.4 Fractal Model

The last model for predicting SSD in my study sites, was done using bedrock fracture spacing and surface point counts data in order to investigate the relationship between fractal patterns and their size distribution collected in the field. Here I used equation (7) to test whether the particle size distributions have a fractal distribution. If they do, the cumulative size distribution plot should be a straight line in log-log space. I also investigate the best fit model by excluding the some of the coarse or fine tails of the model to investigate if the model is more representative of the coarse or finer sizes. I was only able to apply the fractal model to Inyo Creek as this study location was the only one with comprehensive bedrock fracture spacing data available.

4.5 Size Distribution extrapolation

The size distribution data for each my study locations was available in cumulative distribution function (CDF) format. Here, I am also interested in the probability density function (PDF). I also isolated few key percentiles, ($D_{10}, D_{30}, D_{50}, D_{70}, D_{90}$), to be able to represent a full size distribution without tediously calculating CWP and weathering for the full extent of my data set. However, the size distribution provided did not have these specific percentiles that I was looking for, therefore I needed to interpolate to produce uniform percentiles for all the sites. The interpolation formula is as follows:

$$\psi_x = \psi_{low} + \left(\frac{\psi_{high}-\psi_{low}}{P_{high}-P_{low}}\right)(P_x - P_{low}) \quad D_x = 2^{\psi_x} \quad (12)$$

Here, P_x represents the percentile of interest; ψ_{low} represents the nearest low sediment size in Wentworth Phi scale while ψ_{high} represents the nearest high sediment size in Phi scale to the percentile of interest; and P_{high} and P_{low} represent the nearest low and high percentiles to the percentile of interest. Phi scale is a common scale for measuring and categorizing grain sizes. D_x represents the size of sediment at the percentile of interest. Using this interpolation formula, I was able to get the five main percentiles and produce transformation plots for CWP model. The CWP transformation model was produced to compare the initial size distribution to final size distribution at these percentiles in a log-log plot of a power function and see if it agrees with the theory.

5. Results

The results are divided into three separate sections based on the three predictive models, as they are applied to individual study locations. However, as previously mentioned, the fractal model could only be applied to Inyo Creek because of the lack of necessary data for the other two locations. The results are organized to first test the Sklar et al. (2016) theory for predicting the SSD. To do this, I first needed to see if the observed distributions follow the same patterns as expected. After finding some support for CWP model, I used the CWP equation (eqn 1) to estimate degree of weathering for each of the sites. I then tested this weathering parameter to see if it is indeed an explanatory variable for the measured size distributions. This was done by performing multiple regression analysis, combining weathering with other attributes available such as aspect, slope, precipitation, temperature, and erosion rate. Finally, I explored the fractal model using the distribution of bedrock fracture spacing and surface point counts to see if their distribution follows a consistent fractal pattern.

5.1.0 CWP Predictive Model

Sklar et al., 2016 proposed a model for predicting the size distribution that is supplied from hillslopes to channels. Assuming that the initial size distribution provided by the underlying bedrock is known, one can predict the final size distribution based on the strength of chemical weathering ($0 < \text{CWP} < 1$). It should also be possible to use the strength of CWP to estimate the initial size distribution using measured particle size distributions from the field. Also, the last part of this section investigates the sources for the initial sizes. The initial sediment size could be created by bedrock fractures or at a micro-scale by the crystal structure within the lithology. The fraction or percentage of contribution of these two to the initial distribution might be dependent on environmental factors such as elevation or temperature or precipitation. However, the necessary data to perform this analysis was limited only to Inyo Creek.

5.1.1 Inyo Creek

Inyo Creek was the most interesting study location because of the data available. Here, the data is very much tailored for what is needed for the CWP model and thus the Inyo Creek's is the most comprehensive of the three study locations. Inyo Creek has the most sites (18 sites), with the widest elevation difference (2212 m to 2875 m), as well as measurements of bedrock fracture spacing, and mineral crystal sizes for estimating possible initial size distributions.

I first averaged the distribution for bedrock fracture spacing throughout the study location, to use as my initial size distribution. Using the CWP predictive model, I was able to plot the inferred initial size distribution data collected at Inyo Creek, represented by bedrock fracture spacing point counts, against the SSD of all 18 sites to see if their graph follows a pattern similar to what is expected by Sklar et al., 2016. However, the plotted distributions did not perform exactly as expected. The power function in the log-

log space provided by the model did not follow a linear path and started to curve up at the higher percentiles (figure 13). According to the CWP model, the final distributions of sediment supplied to the channel is represented with a straight line, deviating from the middle one-to-one line, in the log-log space, (refer to figure 4). If the line is curved and the distribution drop down much faster than the model predict, which means the model is under-estimating the size reduction of lower percentiles, D_{70} and below. This deviation can be caused by number possibilities. First is that the CWP model is not a good predictive model for finer sediment sizes and perhaps there is physical weathering processes at work which is being ignored. Second is that the initial size distribution provided by only bedrock fracture spacing is not the best representation of the actual input into the hillslope weathering environment. Perhaps the deviation is caused by a combination of both possibilities. Assuming the CWP model is accurate, I moved on to investigate the input of initial size distribution.

One of the main findings of Genetti, 2017 was that, at Inyo Creek, the bedrock fracture spacing distribution does not vary systematically with elevation. This finding was surprising because the median sediment size of individual sites clearly changes with elevation. Higher elevations tend to have coarser median sizes and lower ones have smaller median size. If the initial size distribution is controlled by the distribution of bedrock fracture spacing alone, then, without the influence of weathering, the median size should not change with elevation. Therefore, it is possible that bedrock fracture spacing is only one contributor to initial size distribution and not the sole contributor to the system. If this is so, then there should be an observable trend in initial size distribution that change with respect to elevation. In the next step, I decided to look for such trend and apply the new initial size distribution to my CWP model for Inyo Creek.

One of the concepts discussed by Sklar et al., 2016 is that chemical weathering of bedrock will release mineral size fragments, while physical weathering alone pre-existing

fractures will produce larger fragments. In areas where chemical weathering is more dominant, the mineral crystals would be more pervasive as opposed to physical weathering dominated regions at the peak or ridges. So I needed to account for this variation by investigating the percent contribution of bedrock fracture spacing to local initial size distribution at each of the 18 individual sites and look for any trends with change in elevation, if there are any.

Inyo Creek was the only site with detailed mineral crystal size distribution available, where the landscape is dominated by granodiorite rock with relatively large, up to 5 cm, mineral crystals (Hirt, 2007). I simplified the fraction of mineral crystal contribution to initial size distribution as 'crystal fraction'. I calculated a series of new initial size distributions for Inyo Creek with varying crystal fractions to produce a plot of all possible initial size distributions for each of the 18 sites (figure 14). Because of the large difference in scale of the bedrock fracture spacing and mineral crystal size, the new initial size distribution is bi-modal. This bi-modal distribution is created with weighted summation of the two distribution, where the weight of mineral fraction ranges from 0 to 0.8. Using these new initial size distributions, I was now able to plot each one of the 18 sites against varying crystal fractions from 10% to 80% contribution produced by the weighted sums. My goal was to isolate the plot of crystal fraction that most resembles the expected CWP model prediction (figure 15). This process was done based on two main criteria. First, the resulting plots that crossed the one-to-one line at the middle of the model space were immediately disqualified. This is because that would suggest that parts of final size distribution, after it has been weathered, are larger than they were in the initial distribution, which is generally not possible; with exception of flocculation of fine particles. From the remaining plots, I chose the one that was closest to the expected CWP model prediction for the site.

After associating all sites with a particular initial size distribution, I plotted all the crystal fractions against elevation in order to see if there are any observable trends. The analysis suggested that the initial size distribution input is much more complex than thought before. The crystal fraction contribution to the initial size distribution varies between 70% at lower elevations and 10% at higher elevation (figure 16). This trend seems to be small but nevertheless significant which indicates bedrock fracture spacing contribution increases with an increase in elevation, while crystal fraction contribution decreases with an increase in elevation. After accounting for bedrock fracture spacing contribution to initial sizes, I produced new sets of initial size distribution plots each individual site to see if accounting for crystal fractions did fix the CWP model (figure 17). The CWP model improved significantly where both higher and lower percentiles were near the expected CWP line. However, the median size, D_{50} , was much smaller in field observations than predicted by the model, thus the model fails to predict D_{50} accurately.

Before I concluded my analysis for Inyo Creek, I used the CWP model on all of the 18 individual sites to calculate a CWP derived initial size distribution for each. These new initial size distributions were derived by multiplying individual percentile of observed size distribution with CWP fraction to estimate their initial sizes before they were exposed to chemical weathering and lost some of their mass. After CWP derived initial distributions were produced, I averaged the initial size distribution for all the sites to produce a unified CWP derived initial size distribution to representing the initials for the entire watershed (figure 18). I created this new model output to first plot against observed size distribution and analysis the CWP model from a different perspective. But also, to compare the output with the output produced by crystal fraction plot, to see the deviation of the model, so I can build model a accuracy profile. Overall, the plot of CWP derived initial size distribution and observed size distributions did match the expected

pattern, where the power lines associated with each site were linear in the log-log space and within a reasonable CWP range. Most sites did get finer by the amount expected, with minor deviations at high and low percentiles.

5.1.2 Feather River

For the Feather River location, the analysis followed closely with what I did for Inyo Creek. However, unlike Inyo Creek, here I did not have fracture spacing or mineral crystal sizes to use as possible proxies for the initial size distribution. Instead, Attal et al. (2015) reported a number of landslide point counts within the study location which I used to represent the initial size distribution. I assumed the landslide debris would be the best representative of the size of the material supplied to the surface from below, before erosion, weathering, and biological processes produced the soil as we observe today.

The sample sites in Feather River cluster in three main regions which are closer to each other than the sites at Inyo Creek. The sampling sites chosen by Attal et al., (2015) were clustered to take advantage of the morphology of Feather River's tributary basins, which can be divided into three sections. Due to an accelerated base-level lowering rate from canyon cutting on the main-stem, a knickpoint has developed in this region of Feather River in response (Hurst et al., 2012). The knickpoint is propagating upstream, dividing the hillslopes into the three sections: relict topography above the knickpoint, a hillslope transition zone, and a steepened landscape downstream of the knickpoint (refer to figure 9). The POMD sites are located in the relict topography where erosion rates are relatively low, while FTA sites are located in hillslope transition zone with moderately higher erosion rates, and finally BRC, BRB, and LD are located in steepened landscape where erosion rates are much higher than other sites (Attal et al., 2015).

Assuming the landslide data (LD sites) are the best available representation of the initial size distribution, I decided to average the individual sizes for each of the five

percentiles (D_{10} , D_{30} , D_{50} , D_{70} , D_{90}) to collapse the three landslides into one distribution. Using this distribution, I plotted all 8 sites in log-log space to replicate the CWP model and see if the data follow the expected power trends (figure 19). As shown in figure 19, the most of the observed data fall below the expected CWP line with exception of higher percentiles (D_{70} , D_{90}). Therefore, the CWP model is only able to predict the coarser sizes in this region. This means the model may be missing some aspect of the weathering process that makes smaller particles more susceptible to size reduction in this environment.

Similar to my analysis of the Inyo Creek's data, I used the CWP calculation to estimate the initial size distribution for each Feather River site, and averaged all sites to again produce a single CWP derived initial size distribution. The measured soil data and calculated initial average initial size distribution are plotted in figure 20. With the exception of few minor deviations, the plot approximately follows what is expected. Individual sites have linear power fits associated with them and they are within the chemical weathering window expected. However, similar to Inyo Creek, some of the sites do cross the one-to-one line which should not be occurring. Here, the only discrepancy is where the BRB8-9h's 10th percentile crossed this line. As mentioned previously, crossing the one-to-one line to the top part of the plot would mean the final distribution is larger than the initial, which is not possible. However, all other sites followed the expected CWP trends closely.

5.1.3 Kohala Peninsula

My third study location, Kohala Peninsula in the big Island of Hawaii, had the least amount of data available. There were only 7 sites with measured sediment size. The SSDs were more in-depth than the other two study locations, as each site had detailed distributions representing different soil horizons. However, for the purpose of this research I only needed the average size distribution for the whole sample, which I used.

Also, as mentioned before, there is no data available for initial size distribution at Kohala, and the challenging lithology makes it very difficult to come up with such data.

Moreover, Kohala's data was different than the other two study locations, as one of its sites, the site H7, is located on the other side of the ridge on the windward side of the mountain, while the other 6 sites are located on the leeward side of the mountain. This caused significant differences in precipitation received in H7 compared the rest of the sites.

With limited data available, I was only able to use that data and climatic attributes to calculate CWP for each of the 7 sites and estimate the initial size distribution input. Similar to my analysis of the other two study locations, I used the CWP calculation to estimate the initial size distribution for each the 7 Kohala sites. Much like the other study locations, Kohala's CWP derived plot did mimic what was expected from CWP model, but not as well as the other two study locations. As shown in figure 21, individual sites have linear power fits associated with them and they are within the chemical weathering window. However, the spread of the power line within that window is much wider than the other two locations. The CWP calculated is dependent on the climatic variables such as precipitation and temperature. There is a large difference in precipitation between the sites in Kohala, which is the main cause for this disparity. Also, similar to other locations, some of the sites do cross the one-to-one line which again should not be occurring. They are located in the lower percentiles of the few of the sites, which seems to be a recurring pattern in all the study locations. However, the data points are still very close to the one-to-one line and the variation can be caused by the natural noise in the model.

Overall, the Kohala results were not as promising as the other two study locations. Looking at the position of individual percentiles in the model space, some of the sites (H4, H5, H6) would be better represented with a curve, as their higher percentiles are located much higher on the plot than expected. Here, the model is underestimating size

reduction of D_{50} for higher elevations, and overestimating size reduction of D_{50} for lower elevations. Regardless, there is still a statistically significant agreement between the measured particle size distributions and the patterns predicted by the CWP model for the drier, lower elevation sites.

5.2.0 Multiple Regression Analysis

In the second model I attempted to find the most correlated explanatory variables for the D_{50} for each of the three study locations. By process of systematic search and elimination I isolated the top three attributes that were statistically significant. Finally using the three candidates I constructed an empirical fit model for each study locations to be able to predict D_{50} depending on values of the given variables (attributes). My attributes are comprised of series of topographical, climatic, and calculated attributes that included: aspect, slope, elevation, temperature, precipitation, erosion rate, and the weathering function given in equation 3. Previous studies for each study location suggested different attributes as the main controls on SSD. Therefore, by deriving site-specific empirical fit models, I can test the previous findings and possibly provide additional statistical backing for those claims.

5.2.1 Inyo Creek

Starting with Inyo Creek, I began my analysis by running individual regression on different attributes combined with D_{50} . This way, I got a sense of which attributes are most correlated with the D_{50} and thus I could value those attributes more while doing my multiple regression. The multiple regression analysis was done using stepwise regression, backward elimination technique; where starting with all candidates, the variables are eliminated based on a given model fit criteria until the best fit is achieved. I ranked each potential explanatory variable in descending order of their level of significance in explaining variation in D_{50} , and then eliminated variables from lowest level of

significance until I am left with only variables significant at the 95% confidence level. This process proved more challenging than anticipated. Some attributes that had otherwise lower level of significance and R^2 while running individually, were actually very well correlated when combined with other attributes. This posed a problem, because if two attributes are well correlated to one another, they can inflate each others level of significance.

I decided to use Pearson's R multivariable correlation to find attributes that are co-linear with one another. These variables should not be included together in a multiple regression model. For Inyo Creek, given that precipitation and temperature were derived from elevation, the elevation P-value was inflated when combined with precipitation and temperature (figure 22). Precipitation and temperature should not be selected together as well. After addressing this issue, I was ready for the process of elimination and eventually narrowed the result to aspect, slope, and weathering. This is a bit surprising as Sklar et al., 2016 believed elevation is probably is the main control on D_{50} . However, Leclere, 2016 suggested that aspect is probably is an additional control on D_{50} . Aspect not only was significant, but the most significant attribute in controlling the D_{50} (figure 23). After extracting the y-intercept and individual coefficients, I was then able to use equation (6), to derive the empirical fit model for Inyo Creek:

$$D_{50} = 0.00003 * W^{-1.92} * S^{2.41} * A^{0.28} \quad (13)$$

The multiple regression model explains D_{50} variation in term of weathering function (W), hillslope gradient (S), and local aspect (A), with with P-value of <0.0001 and R^2 of 0.86.

5.2.2 Feather River

Moving on to the second site, I began my analysis by again ranking the attributes based on their level of significant in correlation to D_{50} . I made sure not to include elevation,

precipitation, and temperature at the same time again and proceeded to isolated the top three candidates. Interestingly, the top three most correlated attributes here are identical to Inyo Creek and their level of significance is also of the same order. Once again aspect, slope, and weathering came out on top with aspect being the most significant of the three. For this location however, Attal et al., 2015, suggested that slope is the main control on D_{50} (figure 24). Given that slope is one of the three candidates, the Feather River results do seem to agree with Attal et al., 2015.

I must add that aspect and weathering for Feather River were calculated differently than Inyo Creek. The morphological evolution of Feather River is more complex than Inyo creek. Therefore, the same erosion rate calculations cannot be used for Feather River. I used the cosmogenic radionuclide-derived erosion rates provided by Attal et al., 2015. With erosion rates provided, I was able calculate weathering for each site, which is needed for the empirical fit model. Also the aspect for Feather River was rotated differently than Inyo Creek. Aspect was normalized by 80 degrees of rotation as opposed to 110 degrees. After extracting the y-intercept and individual coefficients, I was able to use equation (5), to derive the empirical fit model for the Feather River study area:

$$\text{Log}_{10}(D_{50}) = -6.08 + 10.49A + 0.84S + 0.72W \quad (14)$$

The multiple regression model explains $\text{Log}_{10}(D_{50})$ variation in term of weathering function (W), hillslope gradient (S), and local aspect (A), with P-value of 0.0002 and R^2 of 0.99. Unlike Inyo Creek, Feather's River's best fit model was based of equation (5) because the attributes used for Feather River's were log transformed, and thus had an exponential relationship rather than a power relationship.

5.2.3 Kohala Peninsula

Lastly, similar to previous study locations, for the Kohala data analysis I began with individual regression analysis on all attributes, and ranked them based on their level of significance. However, other than slope, none of the attributes came out to be significant. After performing stepwise regression and an extensive analysis of the outputs, I noticed that site H3, located in the middle of the elevation transect, is a possible outlier. For this result, I did not include H3 in the analysis, because I determined that it can be excluded as an outlier, using Cook's D technique. After removing H3, slope, aspect, and precipitation were all significant explanatory variables. The R^2 value for aspect was 0.0015, meaning that there remains 99.85% of the variability in D_{50} that is not explained by the empirical model, which is an extremely poor correlation.

Marshall and Sklar, 2012 argued that precipitation is the main control on D_{50} here (figure 25). Given that precipitation was one of the three top candidates for this location, I believe the model is on the right track. Note that unlike Inyo Creek and Feather River, the temperature and precipitation data are not derived from PRISM. Therefore, I would not run into multicollinearity issues with elevation here. The aspect for Kohala was rotated differently from Inyo Cree, but similar to Feather River. Aspect was normalized by 80 degrees of rotation and was only near significant with P-value of 0.056. After extracting the y-intercept and individual coefficients, the most statistically significant model is a power function (eqn 6), to derive the empirical fit model for Kohala:

$$D_{50} = 0.0017 * P^{-1.39} * S^{-5.13} * A^{3.73} \quad (15)$$

The multiple regression model explains D_{50} variation in term of precipitation (P), hillslope gradient (S), and local aspect (A), with P-value of 0.016 and R^2 of 0.99.

5.3.0 Fractal Model

Because of a lack of data for bedrock fracture spacing and point count data for particle size distribution for Feather River and Kohala, I was only able to apply this model to the Inyo Creek data. It is thought that bedrock fractures propagate with a fractal pattern (Roy et al., 2016). Here I try to find patterns in the distribution of bedrock fracture spacing and fracture length to see if there is any relationship that can be used for prediction of fracture spacing's distribution. In theory, if bedrock fractures propagate with a fractal pattern, there should be a linear power relationship for the cumulative distribution of fracture spacing in log-log space. By organizing the bedrock fracture spacing data points from biggest to smallest, in a fractal fashion ($Fracture \geq L$), I was able to plot the bedrock fracture spacing against fractal organization in a log-log space (figure 26). However, I was unable to produce a power linear relationship as needed for this model to work. Instead, fractal model plot is skewed toward the smaller fracture sizes, which means the model's prediction is poor for smaller spacing lengths.

After fractal model failed to predict the pattern of bedrock fracture spacing, I applied the model to the surface point counts data for individual sites. Here I wanted to test this model on the point counts and see if the fractal model is able to predict their distribution. A good predictive model would produce a linear best fit plot in the log-log space. However, again the data points are scattered with a curve, where the data bends down at medium to smaller particle sizes. Observing this trend, I thought perhaps the model is only representative of larger fracture spacing, and thus by excluding smaller sizes, I tried to produce a better fit. While this exclusion seems arbitrary, as long as I am consistent with what data are being excluded I may be able to make a partial predictive model for the larger particle sizes. I decided to exclude all point counts below 2.75 cm in length and test the fit model on individual sites instead. However, after testing this model individually to all surface point counts of each site, I discovered that the curve of scatter

plot for each site changes drastically. Some sites have a curve that is more skewed toward the finer lengths and some were skewed toward coarser lengths (figure 27). That means that by excluding sizes below 2.75 cm, I do not necessary get a good fit model for most of my individual samples.

After many exclusions of data points from both coarser and finer sides of the distribution, it was clear that this model is not very good and cannot reliably predict the distribution of either bedrock fracture spacing or surface point counts. It is likely that they do not propagate fractally and other erosional factors are the dominant control on their distribution. Another possible explanation is that fractal distribution may only be explained with a multifractal model, with one tailored to coarser lengths and one tailored to finer lengths (Perfect, 1997).

6. Discussion

For discussion of results, I first focus on the three predictive models and then discuss what is needed for a more comprehensive future study applying some of these models. The CWP model and the regression analysis look promising as both models manage to predict parts of the sediment size distributions for two out of the three sites. However there are number of physical processes that the models do not account for. I believe there is much more to be achieved with more data, as many of the problems encountered in this research could be caused by the small size of the data sets available. Finally, I discuss the potential of using the CWP and the empirical fit model to improve existing landscape evolution models by proposing a framework for explicitly modeling sediment size produced on hillslopes supplied to the channel. For the landscape evolution model I will use LandLab, a python toolkit for modeling earth surface processes, as an example of simple and user friendly modeling software (Hobley et al., 2017).

6.1 Predictive Models

It is important to note that the CWP is a simple reference model for comparing observation of field data with a mathematically derived function to better understand the impact of chemical weathering on SSD. It is a simplistic generalization of all chemical weathering processes that does not distinguish between chemical reaction rates especially when dealing with multiple minerals within the same distribution. Moreover, CWP model may overlook some physical process that can impact the SSD evolution over time.

The disparity between the observation and predictions could be caused by a number of processes that impact the rate of chemical weathering. For example, the rate of chemical weathering can change depending on the size of individual grains. There is a distinct concave-up pattern that occurs in both the Inyo Creek and Feather River CWP models comparing observed with assumed initial sizes. This concave pattern may be caused by a relatively abrupt change in weathering rate, located around particle size of 10 mm for Inyo Creek and 0.5 mm for Feather River, that produced two separate power linear lines rather than one. Moreover, the disaggregation of mineral crystals by reactions such as hydration can also cause minerals to change, for example feldspar to clay, and thus the chemical weathering rates can change. Therefore, it is possible to improve model accuracy by incorporating different weathering reactions and rates for different particle sizes, and by accounting for varying amount of soluble minerals depending on type of minerals and disaggregation patterns.

Another possible source of variability is the inconsistency of the location of individual sample sites. Ideally, each site would be at the same distance to the channel at any given elevation. While the data from Inyo Creek were collected this way, the data sets from Feather River and Kohala were not collected with this in mind. However, even if all data sets were to be collected at same distance to the channel, there are number of other factors that need to be considered. Depending on topographical attributes such as

slope and aspect and the velocity of the grain based on their size, the residence time for individual particles may differ. With difference in residence time, particles that are located in the same elevation would have a different chemical weathering potential.

Regardless, the CWP model was still able to approximate the variation in particle size distribution for two out of the three study locations. However, it failed to predict the median size (D_{50}) for Inyo Creek and smaller sizes for Feather River. The similarity between the Inyo Creek and Feather River results in prediction of coarse grain sizes indicates that the model may be able to reliably predict D_{70} and D_{90} in landscape similar to that of the Sierra Nevada provided that the right data is available. A noticeable difference between the Feather River and Inyo Creek is the way plots of individual sites are ordered in the log-log space of CWP model. Looking at the plot of Inyo Creek's plot, the size distribution predicted by CWP model seems to be organized in such a way that chemical weathering increases with decrease in elevation. This is due to the fact that generally erosion rates decrease with elevation, and particles spend more time in soil, and this more time in the chemical weathering regime. So it makes sense that with higher elevation, the sediments supplied to the channel would be more closely resemble their initial sizes. Unlike in Inyo Creek, the Feather River erosion rates increase as elevation decreases. That is because the higher elevations are still in the relict topography with low erosion rates and low elevations, while the topography near the river main stem is dominated by steepened slopes. As a result of this morphological dynamic at Feather River, the relationship between D_{50} and elevation is flipped compared to Inyo Creek. So here, it is expected that at higher elevation the size distributions are more shifted toward finer sizes as they are experiencing higher CWP; this is exactly what was observed in figure 19.

The only location where model results are inconclusive is Kohala peninsula of Hawaii, in part because no data were available to independently constrain the input size

distribution. Other limitations for the Kohala analysis include the small number of sampling locations (7), and the basalt bedrock, which may erode differently from the granodiorite that underlies the two Sierra Nevada sites. Future studies with more comprehensive data are needed before we can make a conclusive decision about the CWP model's applicability in wide range of landscapes. For now, the applicability of the CWP model on wide range of landscape with differing lithology is inconclusive.

Multiple-regression analysis shows that aspect was statistically significant in explaining particle size variation at all three study sites. This suggests that the solar radiation has a larger impact on chemical weathering potential than previously recognized. Future research is needed to explore the role of aspect in influencing rates of chemical weathering and particle size reduction on hillslopes. Slope and the weathering function (eqn. 3) were also consistently significant explanatory variables, with the exception of Hawaii, where weathering was not significant. This finding suggests that using the three variables mentioned, it is possible predict D_{50} in different landscapes by constructing an empirical fit model. However, a field campaign to the region of interest is still required to collect the point count data necessary to be able to produce the CWP or the empirical fit model.

The bi-modal distribution of the initial size at Inyo Creek contributed by bedrock fracture spacing and mineral crystal, suggests that bi-modal initial size distributions may be common at other locations as well. Depending on the relative intensities of chemical and physical weathering, the contributions of individual mineral crystals and bedrock fractures producing the initial size distribution can vary. For accurately representing initial size distribution in future studies, this variation in fraction of crystal and fracture needs to be investigated further for possible predictable trends.

6.2 Future Study

Overall, this work highlights the need for additional field data to advance development of models for predicting SSDs on hillslopes. Data are needed for both the hillslope SSD and possible sources of initial size distribution produced from bedrock. The only landscapes where the fit models successfully predicted D_{50} were located in the Sierra Nevada of California, and have similar lithology. Although the geomorphology of Inyo Creek and Feather River are different, the weathering is highly dependent on the activation energy of the more soluble minerals. In order to fully test the capability of the CWP model, there needs to be an additional study with similar data types and conditions as Inyo Creek, but with a different underlying bedrock lithology.

To test for the effects of aspect, future studies need to consider the effect of solar radiation by choosing clusters of sites that have wide variation in solar radiation received. This way the data will be tailored to test aspect as a control on D_{50} while also comparing the SSD among site clusters.

6.3 Landscape Evolution Model Framework

Landscape evolution models are useful tools for simulating and predicting geomorphic processes far into both the past and the future. However, the accuracy of their predictions depends greatly on the parameters that describe the physical process involved in landscape dynamics, particularly erosion and weathering. There are many numerical models available today (Tucker et al., 2001; Coulthard et al., 2002; Slingerland et al., 2008) that encompass a wide variety of earth science disciplines such as river and glacial geomorphology, hydrology, meteorology, and tectonics (CSDMS). The most advanced landscape evolution models combine aspects from all of these disciplines. It is important to know the model frameworks for hillslope sediment size proposed here are

only a segment of the broader picture. By considering evolution of the SSD supplied by hillslopes to channels, one can improve an existing model's predictive accuracy.

Stream channel incision into bedrock is the main mechanism of valley evolution. The relationship between channel incision into bedrock and the sediments supplied by surrounding hillslopes is well established (e.g. Sklar & Dietrich. 2004). Given that sediments provide streams with tools for river-bed abrasion, their size distribution and the amount supplied by hillslopes to channels influences the rate of bedrock incision and longitudinal profile development of the river. In order to accurately predict channel incision, we must understand the factors controlling grain size distribution supplied to the channel by the surrounding hillslopes. Using this knowledge, modelers can account for SSD supplied from surrounding hillslope to the channel.

Numerical landscape evolution models available today, such as LandLab (Hobley et al., 2017), are pixel based. The landscape is divided into many pixels representing a fixed area of land with a set initial elevation (Tucker et al., 2001). As different geomorphic processes erode and modify this computer generated landscape, the pixels either gain or lose elevation. Gain in elevation can come from tectonic uplift while erosion is washing away their top layers and as a result they lose elevation. As the pixels of higher elevation lose sediments, those sediments move to the pixels directly downslope of them, until it reaches the valley bottom where the main channel is located; in which case the sediments are washed away out of the system. While this way of computation may seem complex to some, in reality there are only few simple processes that govern all the pixels' interactions.

Conventional models only have a fixed size distribution, and do not consider the evolution of the size distribution for individual pixels (figure 28). That means, the sediments near the stream channel will have the same distribution as they did near the ridges. If the conventional model was based on a real landscape, each pixel would be

represented by the average distribution observed in the field. This representation of sediment supplied to the channel is clearly not accurate, and therefore the channel incision rates are most likely not realistic. Here I proposed that, using the empirical fit model combined with CWP model, one can estimate the size distribution of individual pixels, and predict their evolution as they approach the stream channel. This estimation can be constructed based on only few real world samples.

If all necessary climatic and geomorphic parameters are known and the model space is already set to represent a real landscape, the numerical model should be able to calculate erosion rates and weathering for each pixel. The dynamic parameters would control pixel evolution more accurately than previous models. Not only would this model have a more realistic pixel SSD, but their size distribution would evolve over time to best represent the topography at every evolutionary step. More realistic sediment supplied to the channel would produce a more realistic channel incision into bedrock and in turn more realistic landscape evolution.

7. Conclusion

In conclusion, the models investigate here supported the hypothesis that hillslope sediment size distributions can be predicted using either the chemical weathering potential model or an empirical fit model derived from multiple regression analysis of significant attributes. By comparing field measurements with model-derived estimates, I was able to test both models applied to a given landscape. The CWP model and the empirical fit model together managed to predict D_{50} , D_{70} , D_{90} accurately, assuming the initial size distribution estimates are accurate as well, while prediction for lower percentiles were poor. This disparity between model results and observations is possibly caused by model simplicity that is not fully representing all physical processes involved. Because of a lack of sufficient data, I was unable to test the models for applicability in a variety of landscape lithologies.

For the best estimate of initial size distribution for each location, I used bi-modally distributed initial sizes with varying contributions from bedrock fracture spacing and mineral crystal sizes for Inyo Creek. I discovered not only that initial size distribution is bi-modal, but the percent contribution from each variable changes with elevation. The higher elevations have larger contribution from bedrock fracture spacing, and lower elevations have more crystal mineral contribution to the input. This input data was unavailable for the other two study locations, with only landslide point counts available in Feather River which I incorporate to represent initial size distribution. Kohala did not have any data on the initial distributions and thus I was only able to plot the sampling data against CWP derived initial size distribution.

I investigated the fractal distribution of Inyo Creek's point counts and bedrock fracture spacing. Assuming the distribution of point count data points represents sediments produced from fractures that propagate fractally, then their distribution should be fractal as well. However, plotting both data sets in log-log space against possible fractal distribution did not produce any the expected power law pattern. I concluded that the fractal model cannot predict the size distribution of both bedrock fracture spacing and surface point counts at Inyo Creek, because either fractures do not propagate fractally or the fractal model cannot explain the full extent of the size distribution with one power fit function.

REFERENCES

- Attal M, Mudd SM, Hurst MD, Weinman B, Yoo K, Naylor M. 2015. Impacts of change in erosion rate and landscape steepness on hillslope and fluvial sediments grain size in Feather River basin (Sierra Nevada, California). *Earth Surf. Dynam.* (3): 201-222
- Burke, B.C., Heimsath, A.M., White, A.F., 2007. Coupling chemical weathering with soil production across soil- mantled landscapes. *Earth Surf. Process. Landforms* 32, 853–873. doi:10.1002/esp.1443
- Chadwick OA, Gavenda RT, Kelly EF, Ziegler K, Olson CG, Elliott WC, Hendricks DM. 2003. The impact of climate on the biogeochemical functioning of volcanic soil. *Chemical Geology* (202): 195-223
- Coulthard, T.J.; Macklin, M.G.; Kirkby, M.J., 2002. A cellular model of Holocene upland river basin and alluvial fan evolution. *Earth Surface Processes and Landforms*, 27, 269–288.
- CSDMS (2018) Modeling tools: https://csdms.colorado.edu/wiki/Main_Page
- Dietrich WE, Bellugi DG, Sklar LS, Stock JD, Heimsath AM, Roering JJ. 2003. Geomorphic transport laws for predicting landscape form and dynamics. *Prediction in Geomorphology* (135): 103–132.
- Dixon, J.L., Heimsath, A.M., Amundson, R., 2009. The critical role of climate and saprolite weathering in landscape evolution. *Earth Surf. Process. Landforms* 34, 1507–1521. doi:10.1002/esp.1836

- Egholm, D. L., Knudsen, M. F., & Sandiford, M. (2013). Lifespan of mountain ranges scaled by feedbacks between landsliding and erosion by rivers. *Nature*, 498(7455), 475-478.
- Genetti J. R. 2017. Evidence for Variation of Hillslope Sediment Size with Elevation at Inyo Creek. Masters Thesis. San Francisco State University.
- Hawaii.gov (2017) Climate data for Hawaii: <http://planning.hawaii.gov/gis/download-gis-data/>
- Hirt, W.H., 2007. Petrology of the Mount Whitney Intrusive Suite, eastern Sierra Nevada, California: Implications for the emplacement and differentiation of composite felsic intrusions. *Geological Society of America Bulletin* 119, 1185–1200. doi:10.1130/B26054.1
- Hobley, D. E. J., Adams, J. M., Nudurupati, S. S., Hutton, E. W. H., Gasparini, N. M., Istanbuluoglu, E. and Tucker, G. E., 2017, Creative computing with Landlab: an open-source toolkit for building, coupling, and exploring two-dimensional numerical models of Earth-surface dynamics, *Earth Surface Dynamics*, 5, p 21-46, 10.5194/esurf-5-21-2017.
- Hurst, M. D., Mudd, S. M., Walcott, R., Attal, M., and Yoo, K. 2012. Using hilltop curvature to derive the spatial distribution of erosion rates, *J. Geophys. Res.*, 117, F02017, doi:10.1029/2011JF002057.
- Langston, A.L., Tucker, G.E., Anderson, R.S., Anderson, S.P., 2015. Evidence for climatic and hillslope-aspect controls on vadose zone hydrology and implications for saprolite weathering. *Earth Surf. Process. Landforms* 40, 1254–1269. doi:10.1002/esp.3718

- Leclere S. 2017. Geomorphic Modeling of Hillslope Sediment Size Distribution Inyo Creek, Eastern Sierra Nevada. Masters Thesis. San Francisco State University.
- Marshall JA, Sklar LS. 2012. Mining soil databases for landscape-scale patterns in the abundance of size distribution of hillslope rock fragments. *Earth Surface Processes and Landforms* (37): 287-300.
- Olyphant, J., Pelletier, J.D., Johnson, R., 2016. Topographic correlations with soil and regolith thickness from shallow-seismic refraction constraints across upland hillslopes in the Valles Caldera, New Mexico. *Earth Surf. Process. Landforms* n/a-n/a. doi:10.1002/esp.3941
- Perfect, E., 1997. Fractal models for the fragmentation of rocks and soils: a review. *Eng. Geol.* 48 (3), 185–198.
- Phillips, J.D., Marion, D.A., Turkington, A.V., 2008. Pedologic and geomorphic impacts of a tornado blowdown event in a mixed pine-hardwood forest. *CATENA* 75, 278–287. doi:10.1016/j.catena.2008.07.004
- PRISM Climate Group (2014) Climate Data. Available at: <http://www.prismclimate.org>., 2016.
- Riebe, C.S., Kirchner, J.W., Finkel, R.C., 2004. Erosional and climatic effects on long-term chemical weathering rates in granitic landscapes spanning diverse climate regimes. *Earth and Planetary Science Letters* 224, 547–562. doi:10.1016/j.epsl.2004.05.019
- Riebe, C.S., Kirchner, J.W., Granger, D.E., Finkel, R.C., 2001. Minimal climatic control on erosion rates in the Sierra Nevada, California. *Geology* 29, 447–450. doi:10.1130/0091- 7613

- Riebe, C.S., Sklar, L.S., Lukens, C.E., Shuster, D.L., 2015. Climate and topography control the size and flux of sediment produced on steep mountain slopes. *PNAS* 112, 15574–15579. doi:10.1073/pnas.1503567112
- Roy SG, Tucker GE, Koons PO, Smith SM, Upton P. 2016. A fault runs through it: Modeling the influence of rock strength and grain-size distribution in a fault-damaged landscape. *J. Geophys. Res. Earth Surf.* (121)
- Schmidt, K.-H., 2009. Hillslopes as Evidence of Climatic Change, in: Parsons, D.A.J., Abrahams, A.D. (Eds.), *Geomorphology of Desert Environments*. Springer Netherlands, pp. 675–694.
- Sklar LS, Dietrich WE. 2004. A mechanistic model for river incision into bedrock by saltation bed load. *Water Resources Research* (40).
- Sklar LS, Riebe CS, Marshall JA, Genetti J, Leclere S, Lukens CL, Merces V. 2016. The problem of predicting the size distribution of sediment supplied by hillslope to rivers. *Geomorphology* (277): 31-49.
- Sklar, L.S., Dietrich, W.E., 2006. The role of sediment in controlling steady-state bedrock channel slope: Implications of the saltation–abrasion incision model. *Geomorphology, The Hydrology and Geomorphology of Bedrock Rivers* 82, 58–83.
- Slingerland, R.L.; Furlong, K.; Harbaugh, J.;, 2008. Simulating Clastic Sedimentary Basins/Physical Fundamentals and Computing Procedures. In: (eds.). 352.
- Stock, G. M., Ehlers, T. A., and Farley, K. A.: Where does sediment come from? Quantifying catchment erosion with detrital apatite (U-Th)/He thermochronometry, *Geology*, 34, 725–728, 2006.

- Stock, G.M., Ehlers, T.A., Farley, K.A., 2006. Where does sediment come from? Quantifying catchment erosion with detrital apatite (U-Th)/He thermochronometry. *Geology* 34, 725–728. doi:10.1130/G22592.1
- Tucker, G.E., Lancaster, S.T., Gasparini, N.M., Bras, R.L., 2001. The channel-hillslope integrated landscape development (child) model. In: Harmon, R.S., III, W.W.D. (Eds.), *Landscape Erosion and Evolution Modeling*. Academic/Plenum Publishers, pp. 349–388.
- West, A.J., Galy, A., Bickle, M., 2005. Tectonic and climatic controls on silicate weathering. *Earth and Planetary Science Letters* 235, 211–228. doi:10.1016/j.epsl.2005.03.020
- Wolfe EW, Morris J. 1996. Geologic Map of the Island of Hawaii. Miscellaneous Investigations Series Map I-2524-A. US Geological Survey: Reston, VA.

Tables

Factors	Initial Size Distribution	Chemical Weathering	Physical Weathering
	Inherited Clast Size Distribution	Mineral Solubility	Differential Heat Stress
	Mineral Grain Size Distribution	Climate: Temperature, Precipitation,	Segregation Ice Growth
	Bedrock Fracture Spacing	Supply of Fresh Mineral Surfaces By Physical Erosion	Bioturbation
	Rock Fracture Toughness		Rock Fall
P(Do) =	f (Lithology, Tectonics)	f (Lithology, Climate, Tectonics)	f (Lithology, Life, Topography, Climate, Tectonics)

Table 1. Controls on hillslope sediment size distribution and evolution.

Sites	Aspect (deg)	Slope (deg)	Precip (mm)	Temp (K)	Elev (m)	Erosion	Weather	D50 (mm)
P2875	108.4	35.7	472.5	272.2	2875	0.230	0.063	13.617
P2862	65.3	28.6	469.6	272.4	2862	0.224	0.065	11.481
P2804	7.6	39.0	456.8	273.3	2804	0.200	0.071	61.891
P2784	6.9	41.6	452.4	273.7	2784	0.192	0.073	40.693
P2676	308.7	45.8	428.5	275.5	2676	0.155	0.085	8.775
P2650	322.8	40.0	422.7	275.9	2650	0.147	0.088	9.375
P2637	33.3	29.2	419.8	276.1	2637	0.143	0.090	11.875
P2582	332.0	35.4	407.7	277.0	2582	0.128	0.097	8.739
P2549	337.5	47.3	400.3	277.6	2549	0.120	0.102	17.499
P2541	325.1	40.8	398.6	277.7	2541	0.118	0.103	8.478
P2447	111.6	31.7	377.8	279.3	2447	0.098	0.117	6.372
P2432	346.0	23.8	374.4	279.5	2432	0.095	0.119	3.420
P2412	94.1	36.9	370.0	279.8	2412	0.091	0.122	8.336
P2350	330.3	32.9	356.3	280.9	2350	0.081	0.132	3.813
P2312	323.6	45.4	349.0	281.4	2317	0.075	0.138	8.489
P2263	320.3	39.2	337.0	282.3	2263	0.068	0.147	1.860
P2230	104.4	25.8	329.7	282.9	2230	0.063	0.153	2.368
P2212	89.0	36.3	325.7	283.2	2212	0.061	0.157	6.266

Table 2. Attribute data for Inyo Creek.

Site ID	Aspect (deg)	Slope(deg)	Precip (mm)	Temp (K)	Elev (m)	Erosion	Weathering	D50 (mm)
POMD2	6.53	12.20	1576.43	287.31	787.18	0.06	0.2922	0.12
POMD4	6.90	15.09	1576.43	287.31	782.97	0.06	0.2922	0.11
POMD6	3.29	13.42	1576.43	287.31	783.41	0.06	0.2922	0.10
FTA1	353.79	25.90	1567.47	288.55	675.65	0.10	0.3225	0.34
FTA9	354.16	28.01	1567.47	288.55	674.58	0.10	0.3225	0.36
BRC3	347.34	46.91	1567.47	288.55	646.62	0.10	0.3225	0.47
BRC0	349.63	24.06	1567.47	288.55	677.06	0.10	0.3225	0.22
BRB8-9h	356.91	42.74	1567.47	288.55	637.45	0.10	0.3225	1.18

Table 3. Attribute data for Feather River

Sies	Aspect (deg)	Slope (deg)	Precip (mm)	Temp (K)	Elev (m)	Erosion	Weathering	D50 (mm)
H7	341.260	4.560	3193.600	286.110	1254.000	0.220	0.355	0.026
H6	178.630	3.930	1322.980	286.970	992.000	0.141	0.248	0.022
H5	214.750	4.910	1043.530	287.570	792.000	0.100	0.232	0.009
H4	256.120	6.540	721.820	288.670	674.000	0.082	0.207	0.014
H3	228.240	4.820	314.600	290.790	356.000	0.048	0.157	13.470
H2	233.860	2.200	246.660	291.960	185.000	0.036	0.149	9.525
H1	259.760	4.680	226.900	292.350	77.000	0.030	0.146	0.314

Table 4. Attribute data for Kohala Peninsula

Percentile	P2875	P2862	P2804	P2784	P2676	P2650	P2637	P2582
10	1.954	0.624	14.166	2.783	1.051	1.057	1.163	1.080
30	5.837	5.586	28.361	15.057	2.993	3.062	4.802	3.327
50	13.617	11.481	61.891	40.693	8.775	9.375	11.875	8.739
70	96.363	38.023	233.154	66.427	77.210	118.027	30.288	15.693
90	342.563	193.753	455.233	183.783	316.635	281.497	319.691	342.534



Percentile	P2549	P2541	P2447	P2432	P2412	P2350	P2312	P2263	P2230	P2212
10	1.578	3.386	0.935	0.850	1.507	0.859	1.195	0.737	0.761	0.997
30	7.755	7.158	2.032	1.980	5.141	1.631	2.894	1.268	1.405	2.439
50	17.499	8.478	6.372	3.420	8.336	3.813	8.489	1.860	2.368	6.266
70	34.157	11.315	17.687	73.273	146.670	35.036	110.496	3.346	4.601	10.732
90	329.786	28.496	401.235	371.791	719.764	127.531	296.623	77.997	9.383	691.751

Tables 5. Five percentiles (10, 30, 50, 70, 90) for Inyo Creek's point count size distributions.

Percentile	P2875	P2862	P2804	P2784	P2676	P2650	P2637	P2582
10	2.188	0.643	18.893	3.263	1.151	1.162	1.293	1.202
30	7.086	6.784	40.036	20.359	3.633	3.754	6.193	4.204
50	17.595	14.719	93.132	59.833	11.844	12.888	16.836	12.317
70	143.827	53.337	391.082	101.791	129.180	210.375	47.352	23.632
90	561.386	307.157	806.579	306.855	608.965	548.515	639.324	731.018



Percentile	P2549	P2541	P2447	P2432	P2412	P2350	P2312	P2263	P2230	P2212
10	1.846	4.349	1.043	0.938	1.811	0.962	1.419	0.815	0.850	1.175
30	10.956	10.057	2.522	2.460	7.374	2.018	3.976	1.543	1.758	3.409
50	27.228	12.155	9.251	4.587	12.819	5.392	13.921	2.421	3.265	10.479
70	57.537	16.795	29.534	150.954	340.92	70.214	276.447	4.834	7.176	19.885
90	726.886	47.251	1027.933	961.589	2103.9	313.128	873.089	197.037	16.703	2832.842

Percentile	Average	stdev	CV
10	2.4135	4.0955	1.6969
30	7.2965	9.1607	1.2555
50	17.9727	22.2284	1.2368
70	109.5500	117.3564	1.0713
90	717.0410	701.7137	0.9786

Tables 6. Five percentiles (10, 30, 50, 70, 90) for Inyo Creek's CWP derived initial size distributions.

Percentiles	POMD2	POMD4	POMD6	FTA1	FTA9	BRC3	BRC0	BRB8-9h	LD1	LD2	LD3
10	0.0048	0.0041	0.0039	0.0134	0.0115	0.0108	0.0094	0.0424	0.35	0.6	0.275
30	0.0336	0.0292	0.0246	0.1088	0.1000	0.1016	0.0744	0.257	9.105	26.360	6.100
50	0.1221	0.1133	0.0963	0.3415	0.3604	0.4671	0.2188	1.181	34.947	66.161	46.406
70	0.4203	0.4470	0.8943	1.1204	1.5417	1.9265	1.1023	3.040	90.403	93.125	85.276
90	1.5797	1.6812	2.1935	2.5711	68.8440	7.7413	2.7491	11.778	168.098	145.782	154.838

Tables 7. Five percentiles (10, 30, 50, 70, 90) for Feather River's sediment size distributions.

Percentiles	POMD2	POMD4	POMD6	FTA1	FTA9	BRC3	BRC0	BRB8-9h	LD1	LD2	LD3	Average	stdev	CV
10	0.0069	0.0057	0.0054	0.0264	0.0218	0.0202	0.0168	0.1126	1.6753	3.3169	1.2341	0.0270	0.0355	1.3169
30	0.0749	0.0630	0.0510	0.3687	0.3316	0.3385	0.2283	1.0873	104.132	400.543	62.677	0.3179	0.3377	1.0623
50	0.3659	0.3339	0.2734	1.5590	1.6686	2.3137	0.8895	7.4454	572.58	1285.65	820.22	1.8562	2.3770	1.2806
70	1.6698	1.8010	4.2223	6.9701	10.422	13.800	6.8283	24.527	1909.62	1982.76	1773.41	8.7802	7.5876	0.8642
90	8.4927	9.1681	12.7108	19.8552	1251.16	79.651	21.603	135.170	4191.10	3498.94	3776.63	192.2266	430.2143	2.2381

Tables 8. Five percentiles (10, 30, 50, 70, 90) for Feather River's CWP derived initial size distributions.

Percentile	H7	H6	H5	H4	H3	H2	H1
10	0.0015	0.0014	0.0013	0.0013	0.0029	0.0034	0.0026
30	0.0058	0.0046	0.0021	0.0024	0.0322	0.0657	0.0166
50	0.0259819	0.0216000	0.0089633	0.0138191	13.4703842	9.5250000	0.3144703
70	0.0977	0.1176	0.0534	6.2822	32.0227	28.3700	24.2109
90	0.3918	2.0000	19.0500	40.9411	56.7814	64.1774	71.4351

Tables 9. Five percentiles (10, 30, 50, 70, 90) for Kohala's sediment size distributions.

Percentile	H7	H6	H5	H4	H3	H2	H1	Average	stdev	CV
10	0.0019	0.0016	0.0014	0.0014	0.0036	0.0043	0.0030	0.0025	0.0012	0.4776
30	0.0175	0.0079	0.0027	0.0030	0.0621	0.1381	0.0271	0.0369	0.0492	1.3320
50	0.1977	0.0637	0.0179	0.0281	81.3861	48.4540	0.8534	18.7144	32.9663	1.7615
70	1.6971	0.6287	0.1867	66.7159	227.9142	175.1792	139.6548	87.4252	94.0640	1.0759
90	16.1720	28.9772	424.6628	721.4516	450.3775	458.0928	497.1982	370.9903	257.6789	0.6946

Tables 10. Five percentiles (10, 30, 50, 70, 90) for Kohala's CWP derived initial size distributions.

Figures

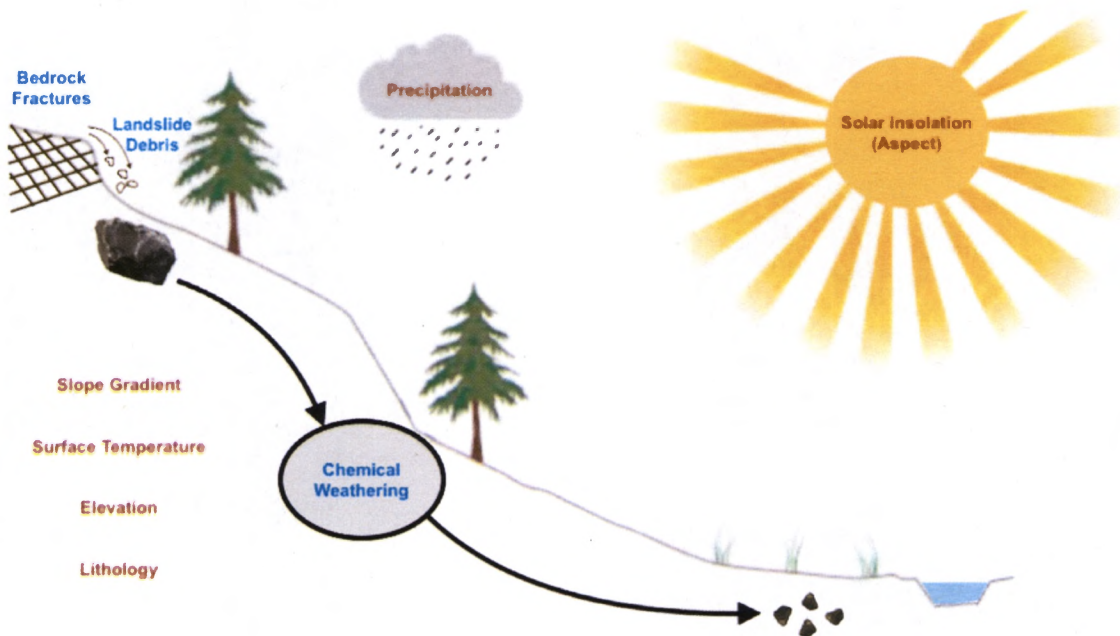


Figure 1. Geomorphic and climatic attributes such as precipitation, temperature, aspect, slope, elevation and lithology are controls on chemical weathering potential. The debris produced by bedrock disaggregation through bedrock fracturing and landslide are the input into the system, where rock particles get finer while exposed to the chemical weathering regime.

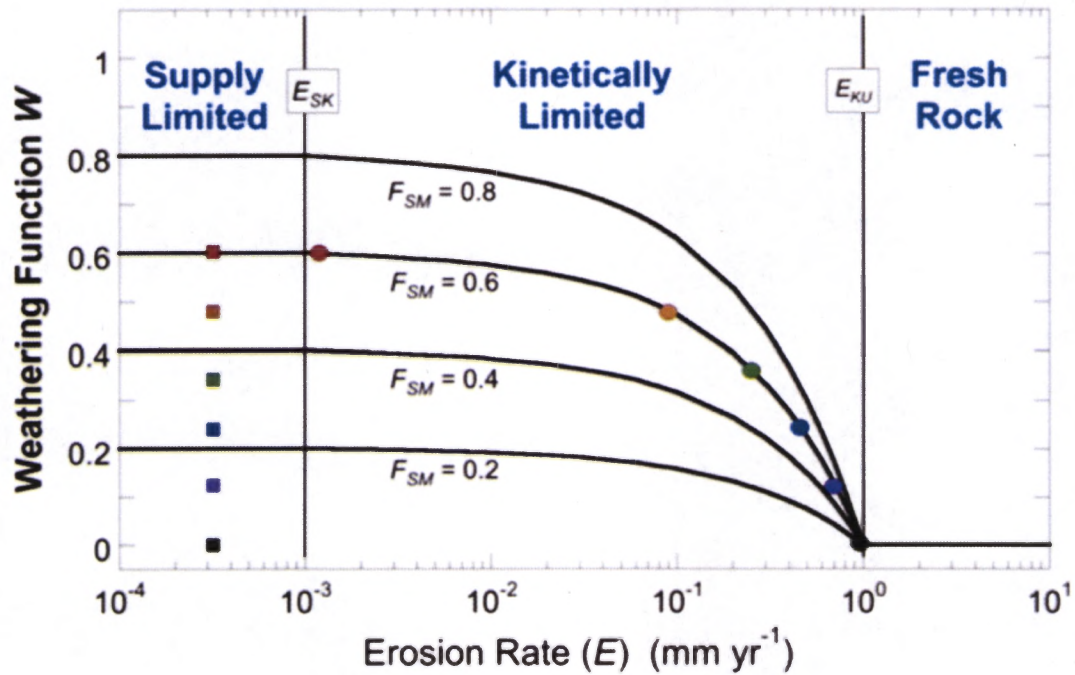


Figure 2. Influence of erosion rate on weathering regime is divided into three different scenarios. First, when the erosion rates are low, weathering is limited by the supply of fresh minerals, and only depends on the chemical weathering potential (CWP) and fraction of soluble minerals (F_{SM}). Second scenario is where erosion rates are intermediate and weathering is limited by the residence time of sediments particle in the chemical weathering regime. The final scenario is when erosion rates are so high that chemical weather has no time to operate and thus chemical weathering is negligible (Sklar et al., 2016).

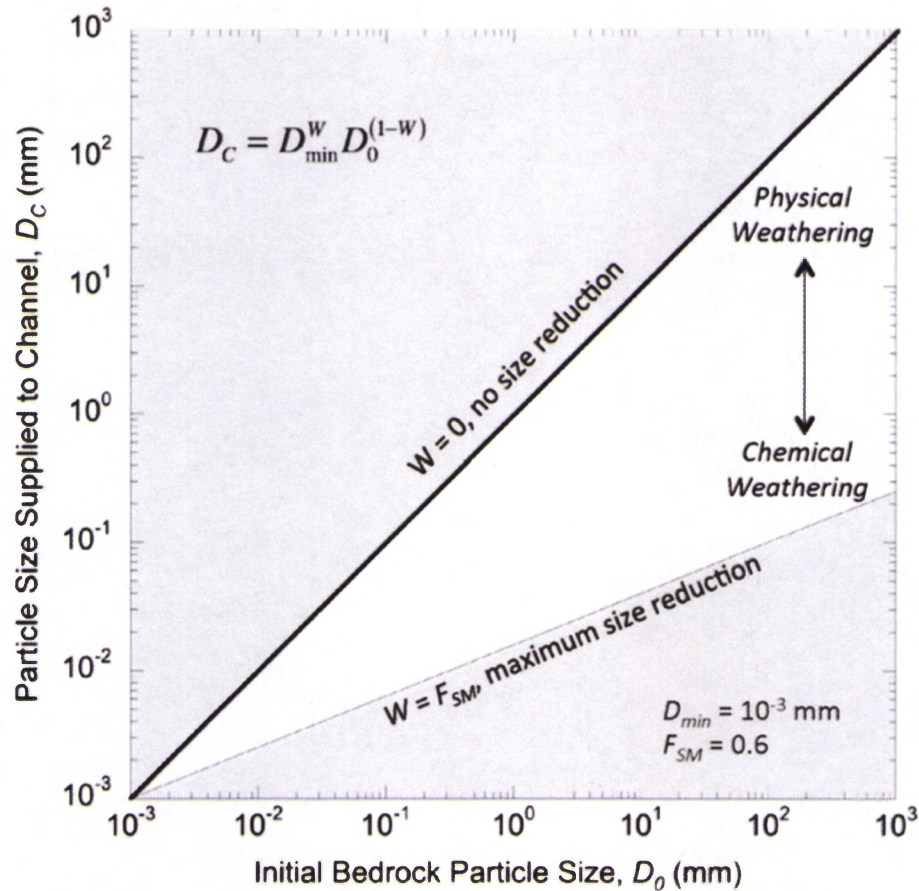


Figure 3. Modeling framework for the CWP model in a log-log space. In the model space, initial size distribution (D_0) can be transformed into the size distribution that is supplied to the channel (D_C), using the transformation power equation (eq. 4). The plot is divided in half with a one-to-one line, representing when no size reduction has occurred $W = 0$. The maximum chemical weathering possible when $W = F_{SM}$, where weathering gets supply limited. These two lines provide a maximum range for the CWP's size transformation. Outside of the bounds of CWP, physical weathering is more dominant. The model parameter D_{min} also represents the smallest relevant particle size for this research (Sklar et al., 2016)

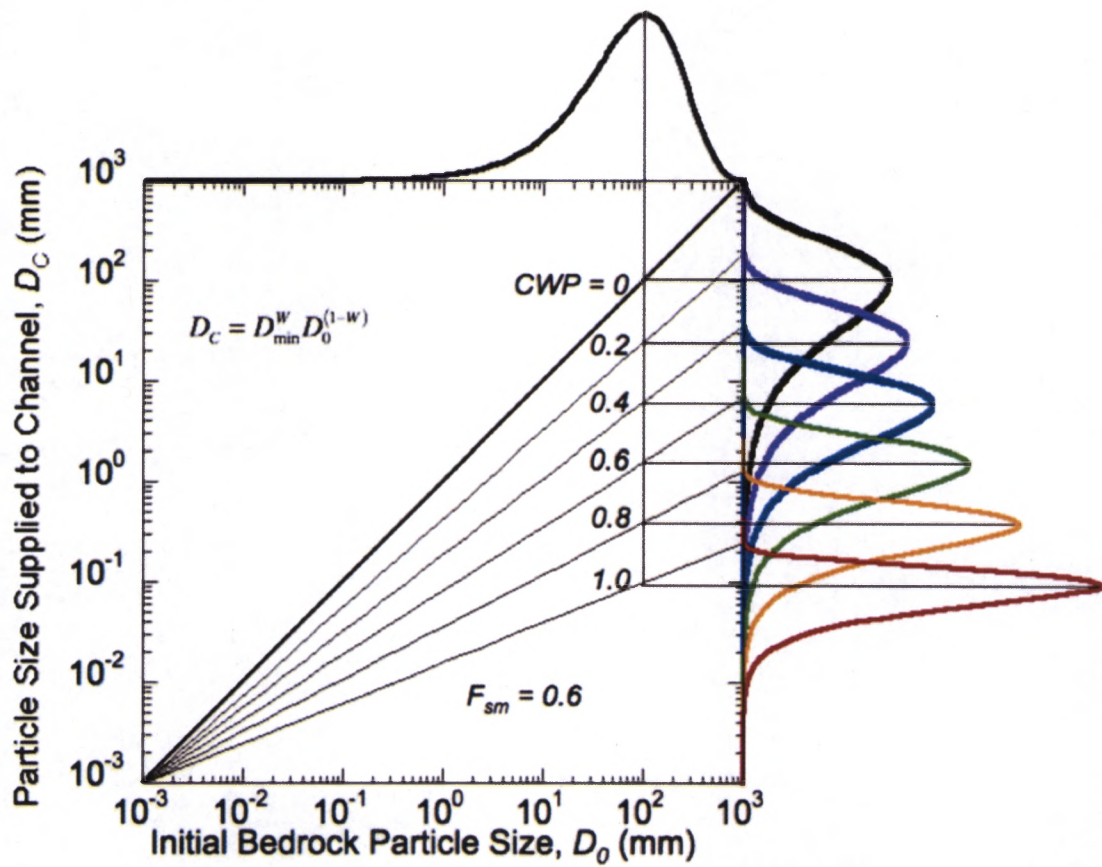


Figure 4. CWP model for particle size transformations across a range of chemical weathering potential. The black curve on the upper horizontal axis represents the initial particle size distribution by mass and is assumed to be exponential. The colored curves on the right vertical axis are transformed size distributions for chemical weathering potential values that range from no weathering (0) to maximum weathering (1.0), where the fraction of soluble minerals is 0.6. The thin black lines are transformations of distribution mode (Sklar et al., 2016).

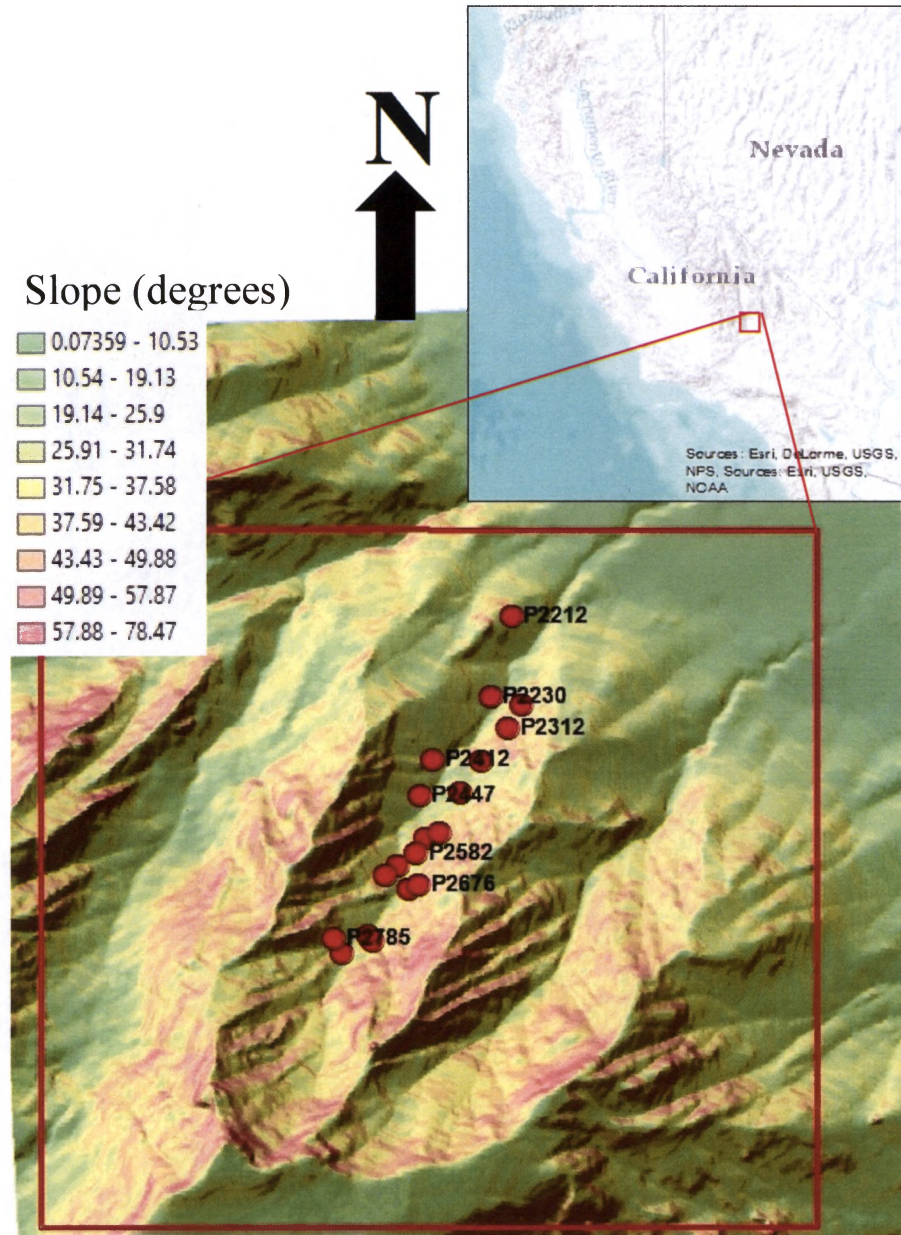


Figure 5. First study location (Inyo Creek). Positioned to the northeast facing side of Mount Whitney, it is part of the southern Sierra Nevada. Predominant lithology is granodiorite. Point count locations are represented by the letter P followed by site's elevation from sea level.

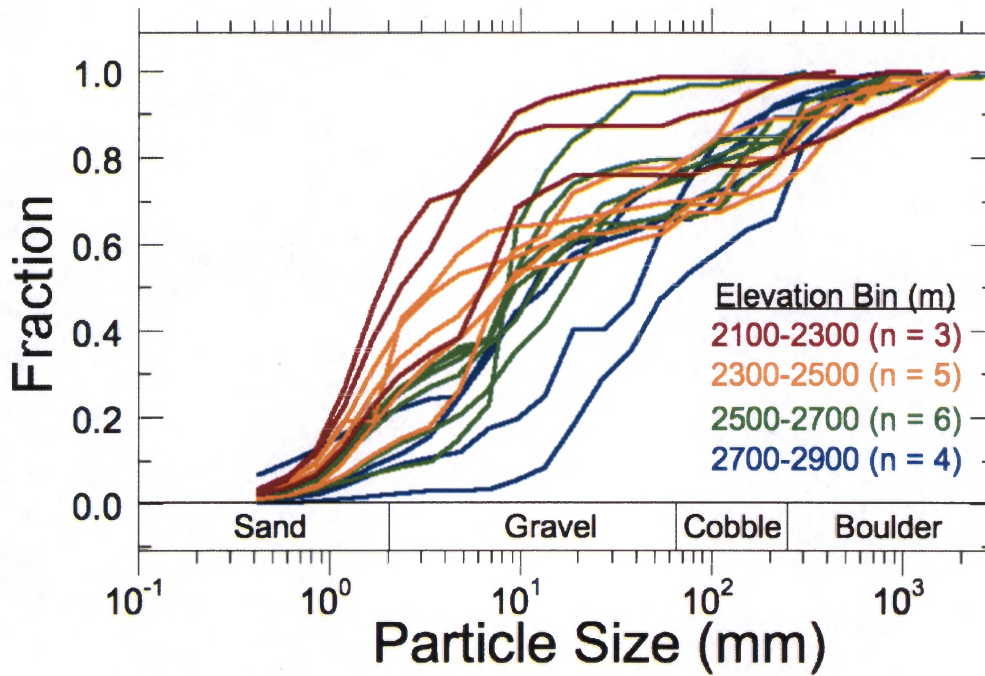


Figure 6. The cumulative particle size distributions of complete point counts for Inyo Creek is shown. The Complete point count distributions includes point count and bulk data. Colors represent a range of elevations from higher elevation (blue) to lower elevation (red) (Genetti, 2017).

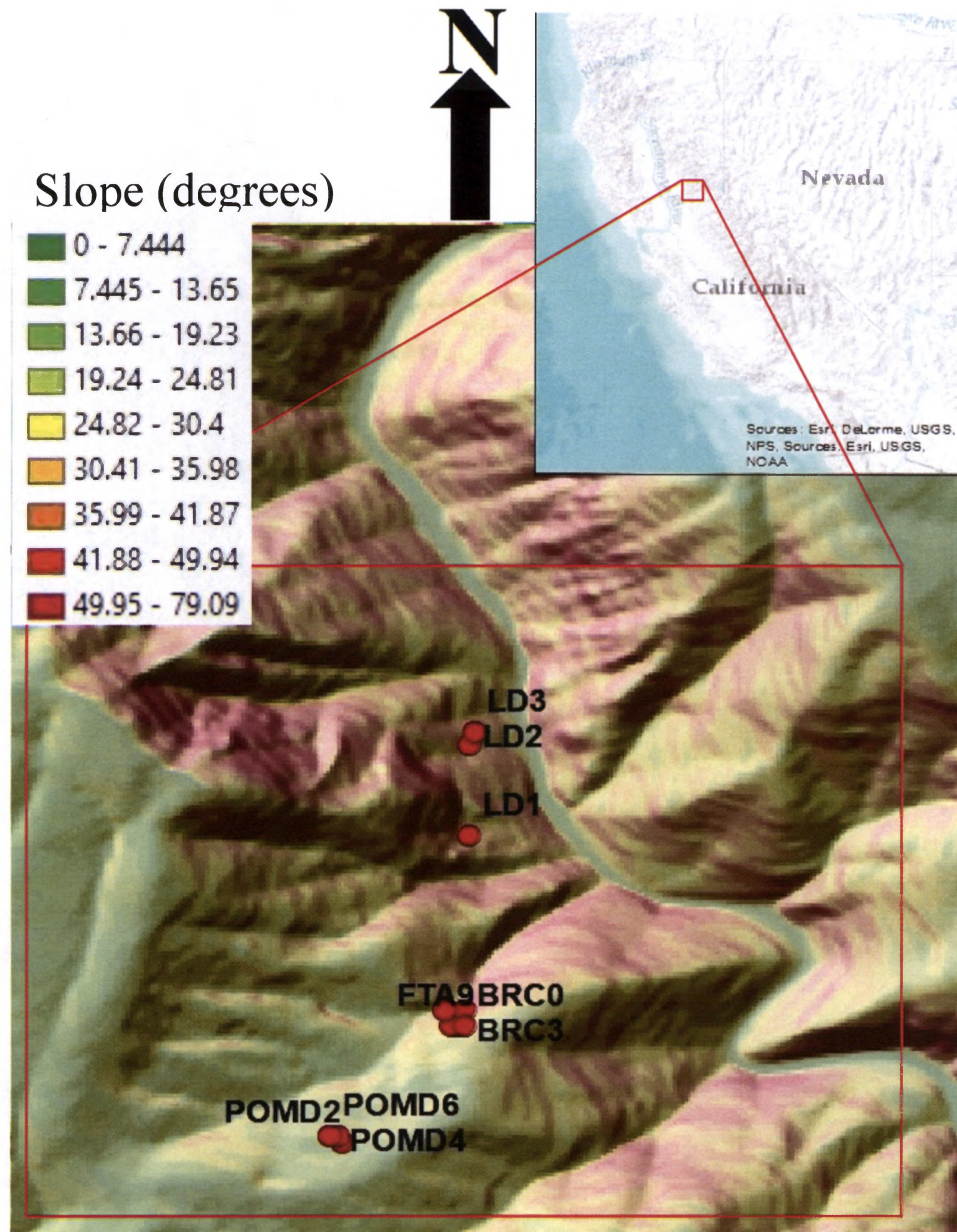


Figure 7. Second study location (Feather River) is located mostly within the watershed boundary of one of Feather River's tributaries called Bald Rock. Although, the landslide sediments (LD) are not within the watershed of Bald Rock. Feather River is located in northern Sierra Nevada, predominantly lithology is Tonalite and Granodiorite.

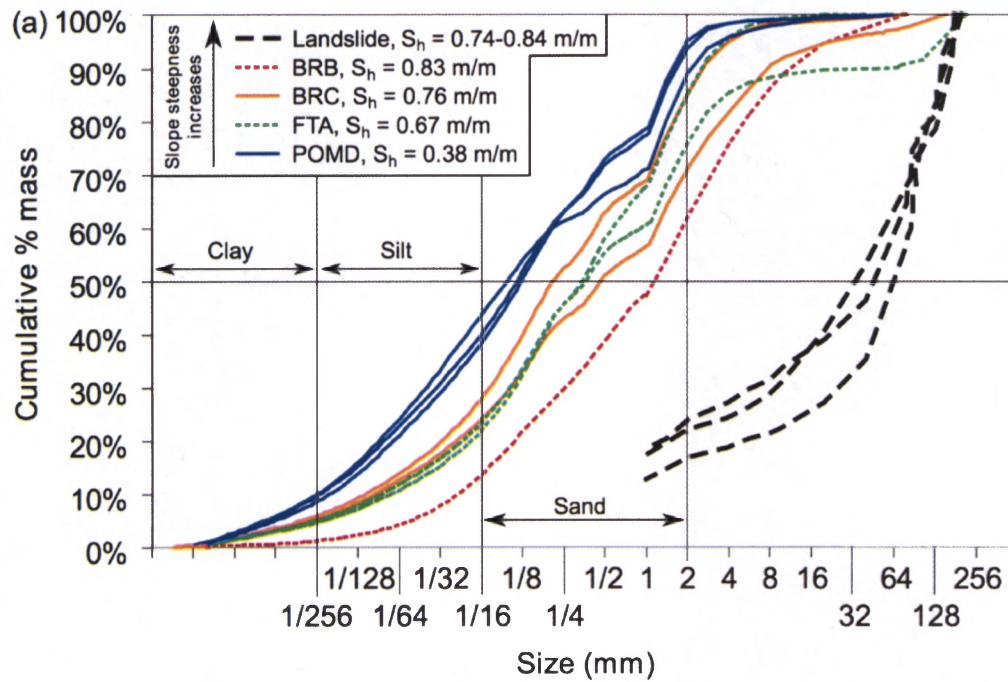


Figure 8. Cumulative grain size distributions measured for the sources of sediment in Bald Rock basin. Line colors reflect the steepness of hillslope gradient (S_h) from blue (least steep) to black (the steepest). Note the log₂ scale on the x axis (Attal et al., 2015).

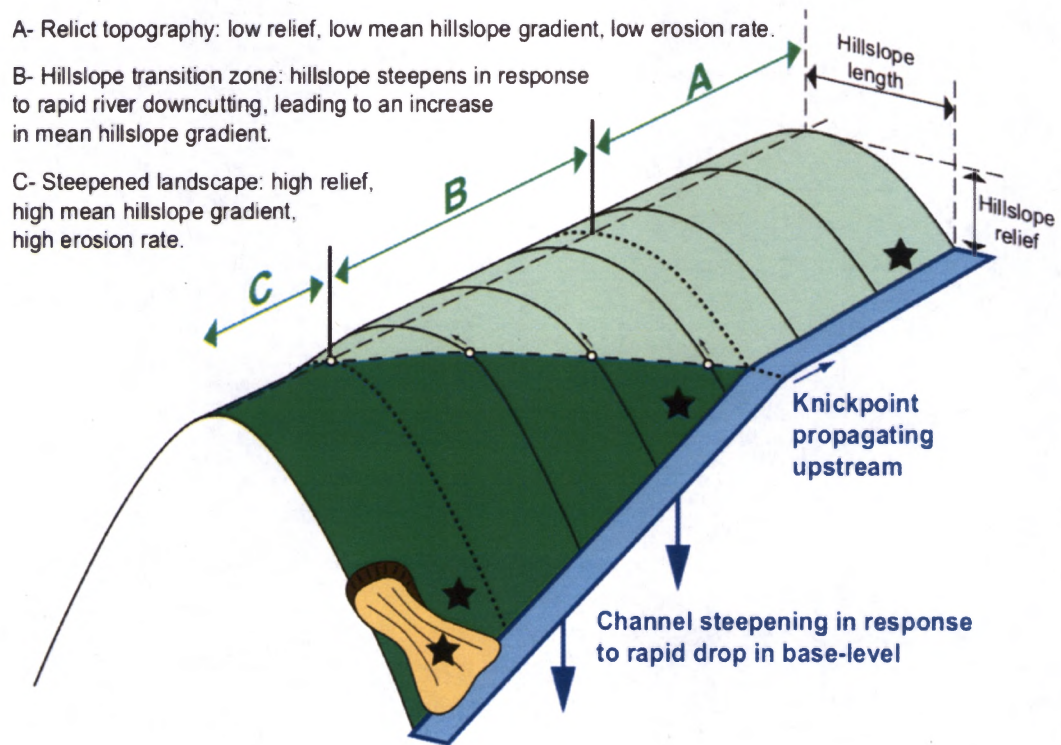


Figure 9. Schematic illustrating of geomorphology of Bald Rock tributary adapted from (Hurst et al., 2012). As a result of local uplift and rapid drop in base level, a knickpoint has developed in Feather river that is propagating upstream along the channel. This condition has created three separate distinct topographies. The stars shown above represents samples from each of the three regions and samples from landslide debris nearby. The three regions identified as: (A) relict topography above the break in slope (POMD), (B) in the transition zone where the hillslopes have not completely adjusted to the base-level fall (FTA), and (C) below the break in slope (BRC and BRB) (Attal et al., 2015).

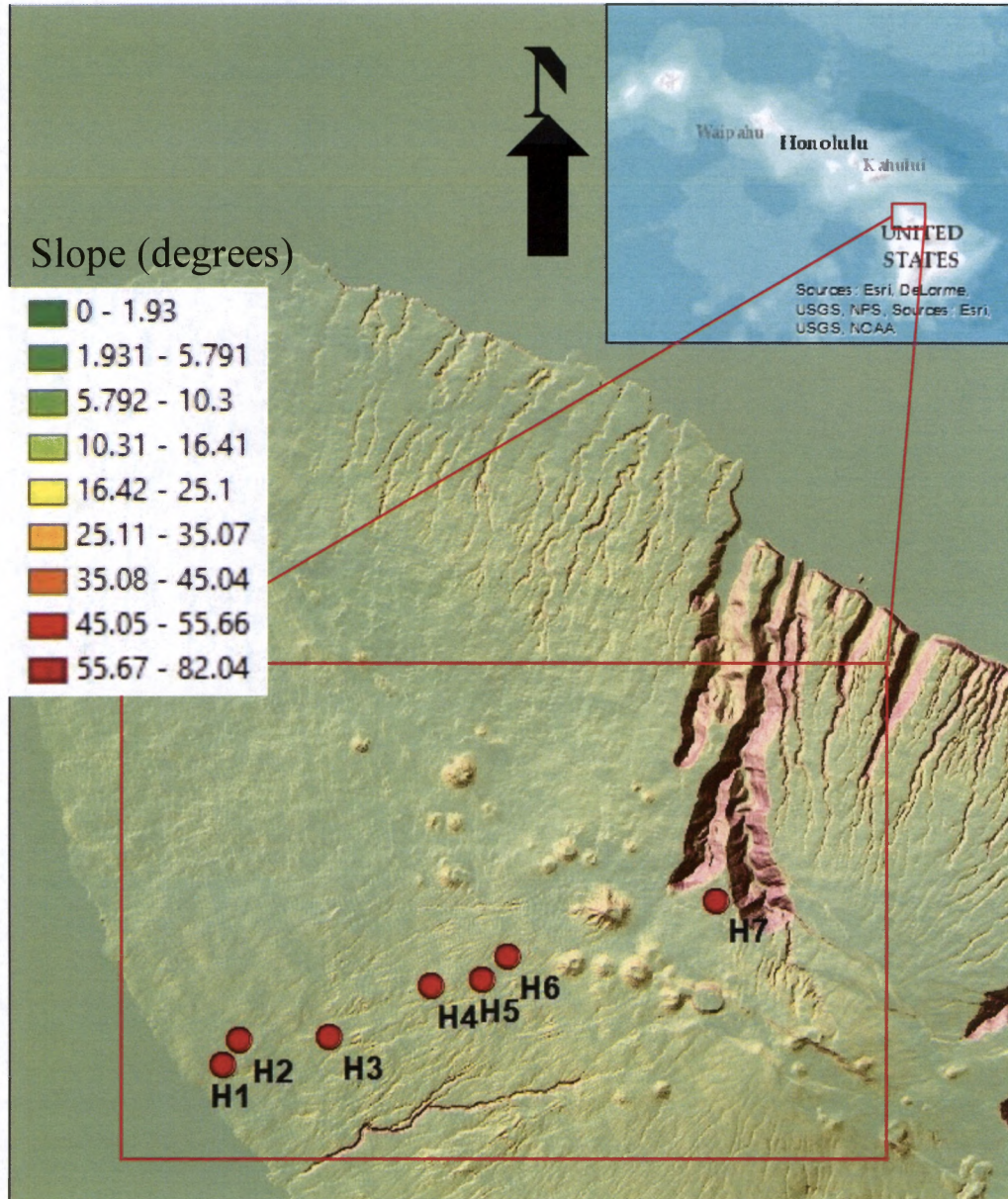


Figure 10. Third study location (Kohala Peninsula). Positioned in the northern part of big island of Hawaii. Sites are identified as (H#), while most sites are located in the south facing part of the Kohala mountain, the site H7 is located over the ridge on the north facing side of the mountain. Kohala's climate changes dramatically from wet north facing side to arid, desert like, south. Predominant lithology is basalt.

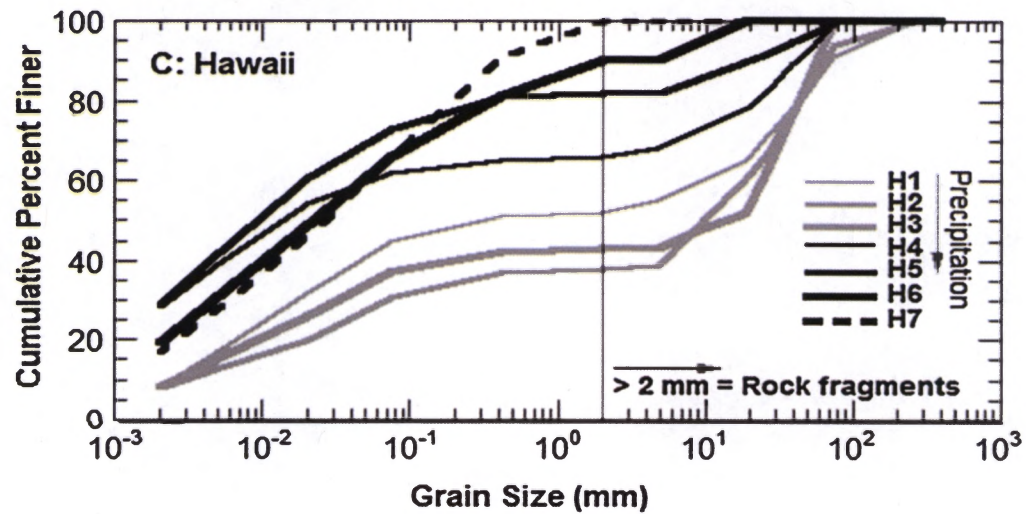


Figure 11. Cumulative grain size distributions measured for the sources of sediment in Kohala. The different shades of grey are organized based on amount of precipitation received, H1 least to H7 most precipitation (Marshall & Sklar, 2012).

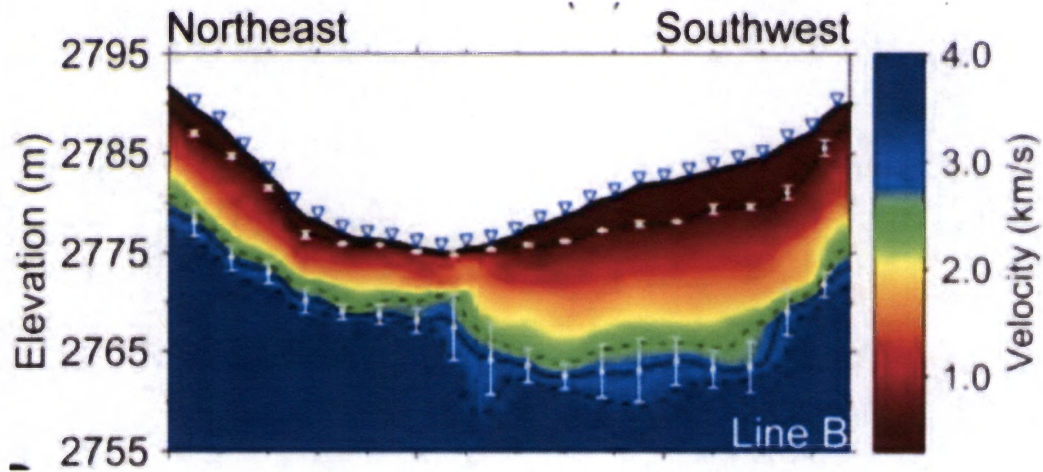


Figure 12. Aspect's effect on sediment size distribution. Cross section of valley in Arizona from previous study, indicating north-facing slopes have greater soil depth compared to south facing ones (Olyphant et al., 2016).

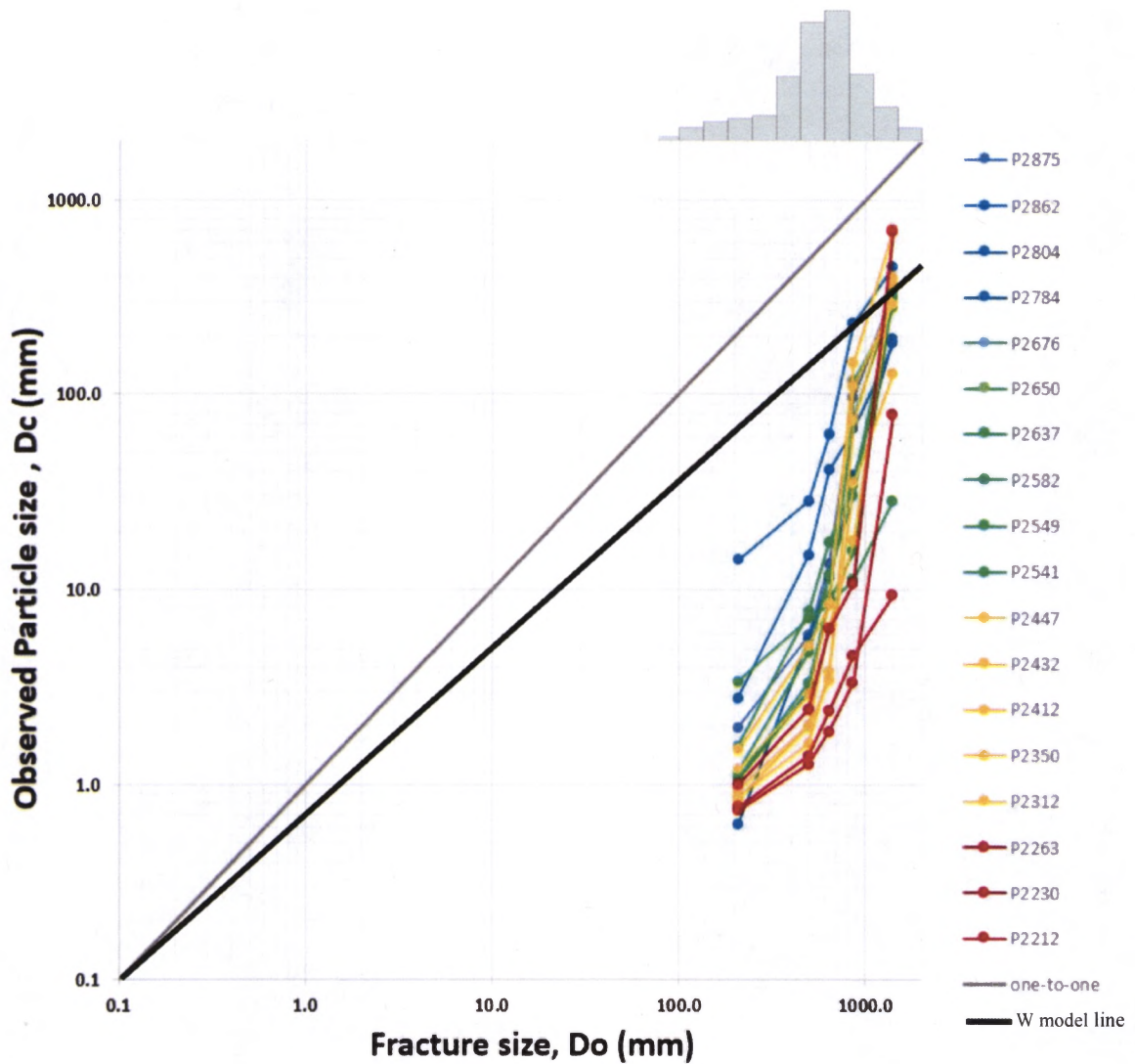


Figure 13. Inyo Creek's first CWP model for particle size transformations across a range of chemical weathering potential, using bedrock fracture spacing as the only input. Colors correspond to the range in elevation with red being the lowest and blue the highest. Gray line crossing the middle is the one-to-one line where no chemical weathering has occurred and the size distribution hasn't changed.

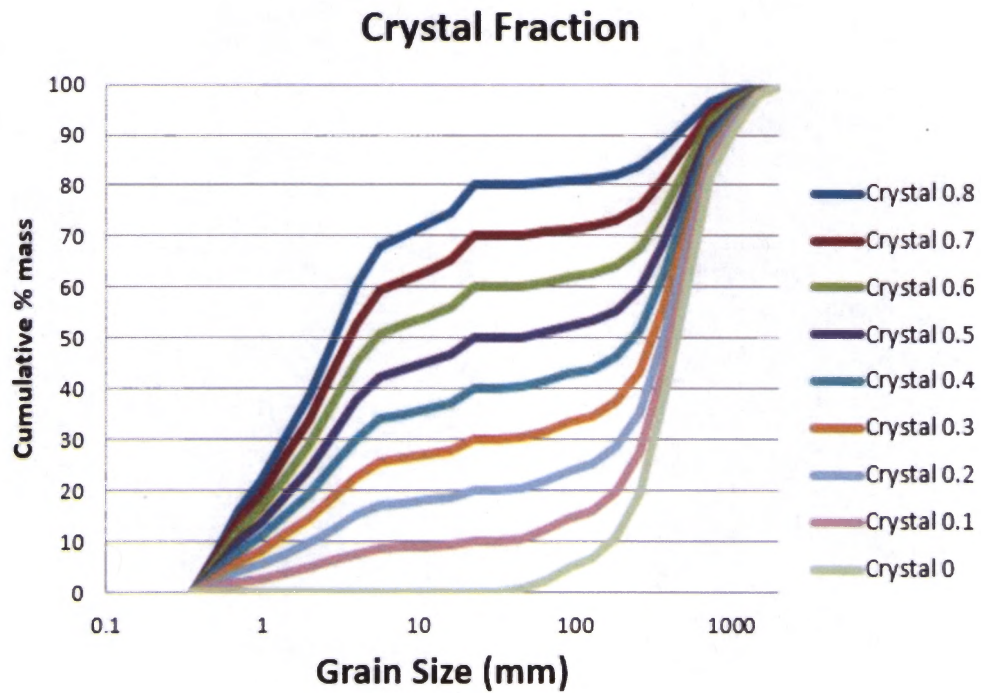


Figure 14. Percent contribution of mineral crystals by mass to the initial size distribution ranging from 0 to 80%. E.g. Crystal 0.8 represents 80% of initial size distribution is originated by mineral crystals and 20% by bedrock fracture spacing.

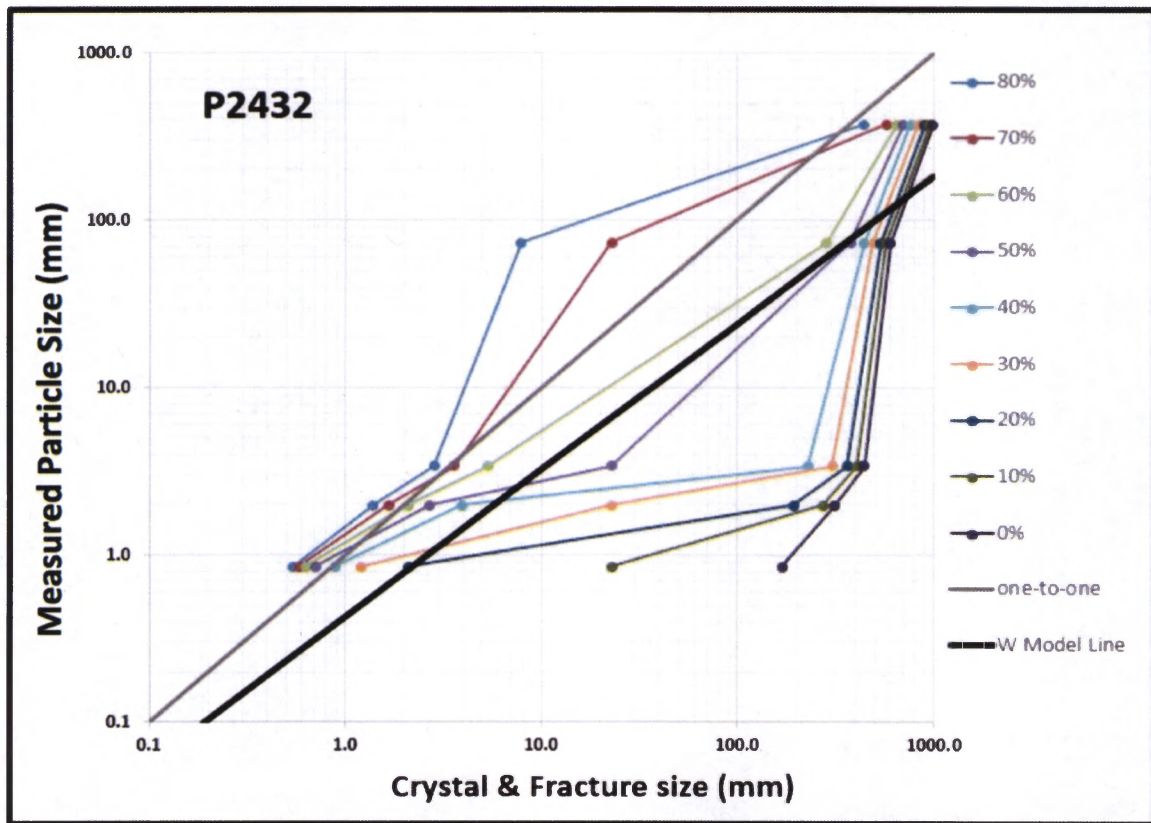


Figure 15. Sample CWP model with varying crystal fractions. Each of the 18 sample sites, (site P2432 shown here), were plotted against all the possible crystal fractions (0 to 80% range) in order to find the best fit model for the CWP in the given site. The thick black line is the expected size distribution given the local CWP. Grey line in the center is the one-to-one line, any distribution that crosses the gray line would imply the final distribution is larger than the initial, which is not possible.

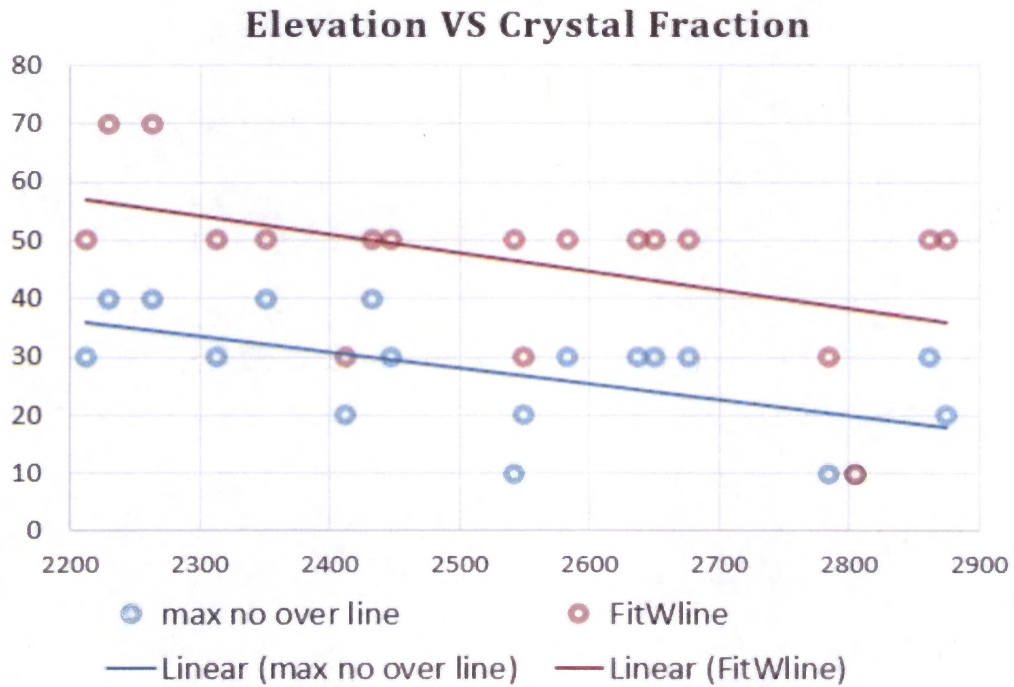


Figure 16. A plot of all the best percentage crystal fraction for all of Inyo Creek's sampling sites. Crystal fractions show a trend with respect to elevation. Higher elevations seem to have lower percent of crystal fraction contribution to the initial size distribution. The redline represents the percentage of crystal fraction that produced to most linear distribution in the CWP model's log-log space. The blue represents the maximum distribution that did not cross the one-to-one line in the CWP model's log-log space.

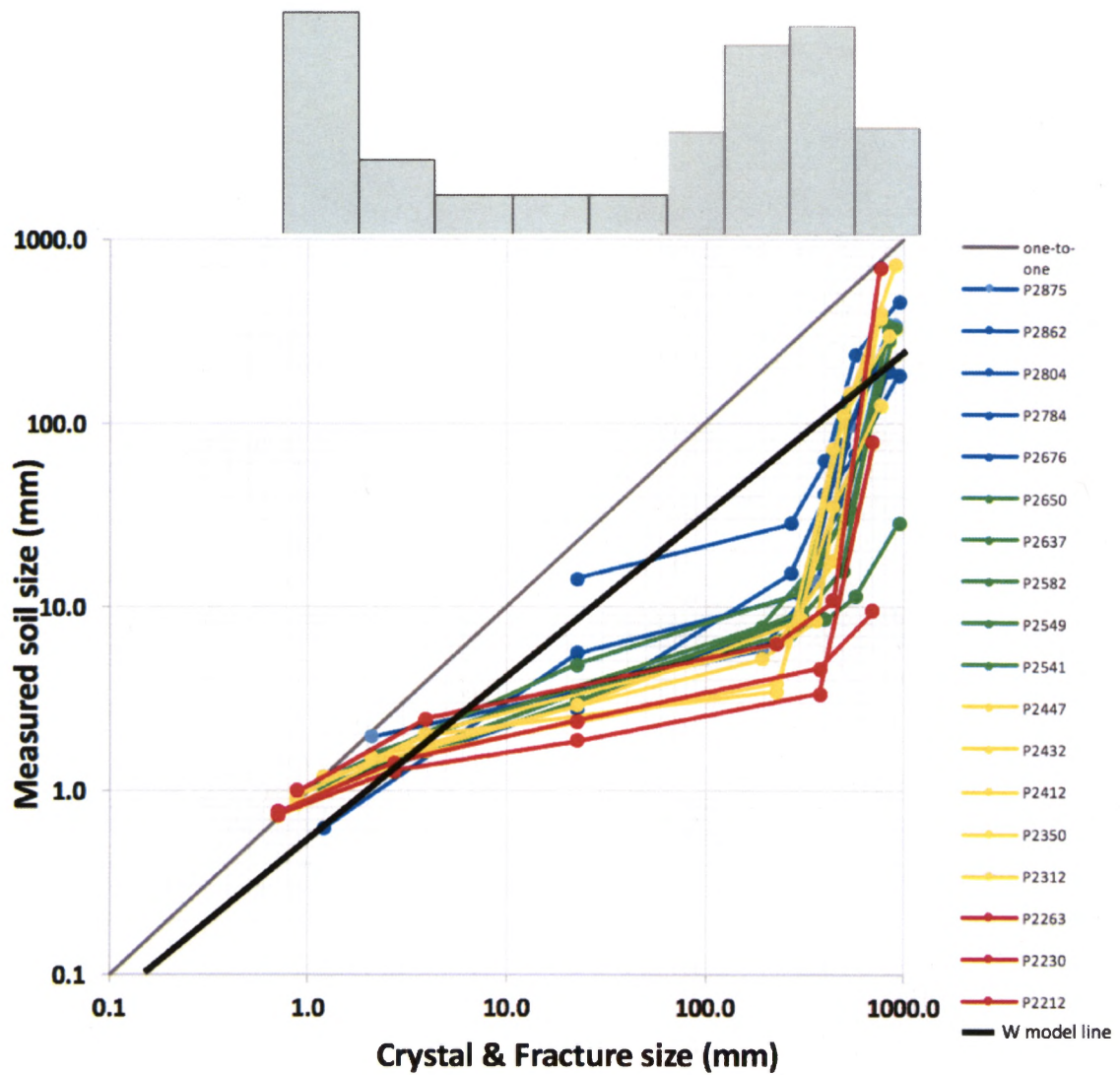


Figure 17. CWP model with the bi-modal initial distribution, represented with the best crystal fraction percentage for individual sample sites. Colors correspond to the range in elevation with red being the lowest and blue the highest. Gray line crossing the middle is the one-to-one line where no chemical weather has occurred and the size distribution hasn't changed.

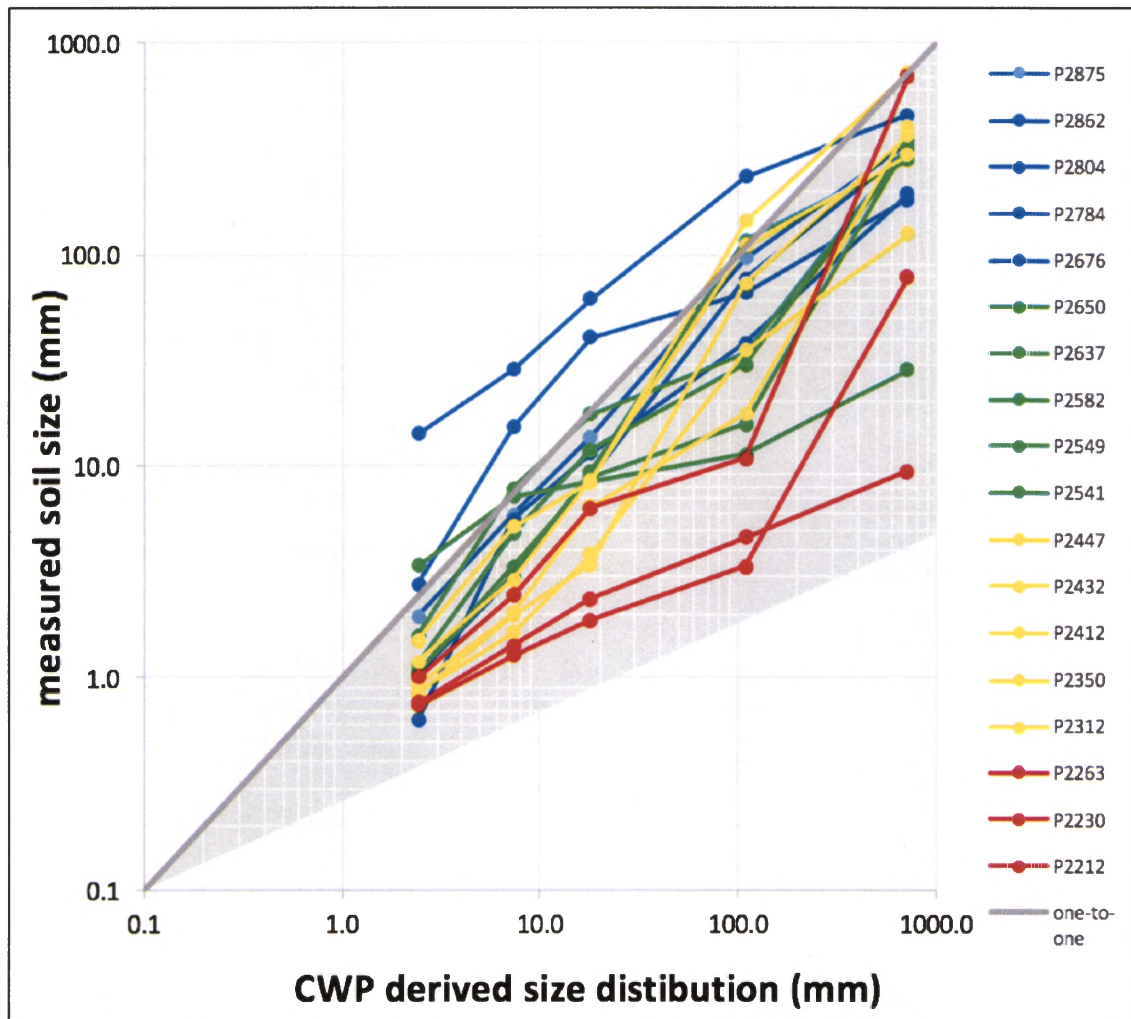


Figure 18. Individual sample sites plotted against CWP derived initial size distribution. Two of the distributions from the high elevation are mostly above the one-to-one line.

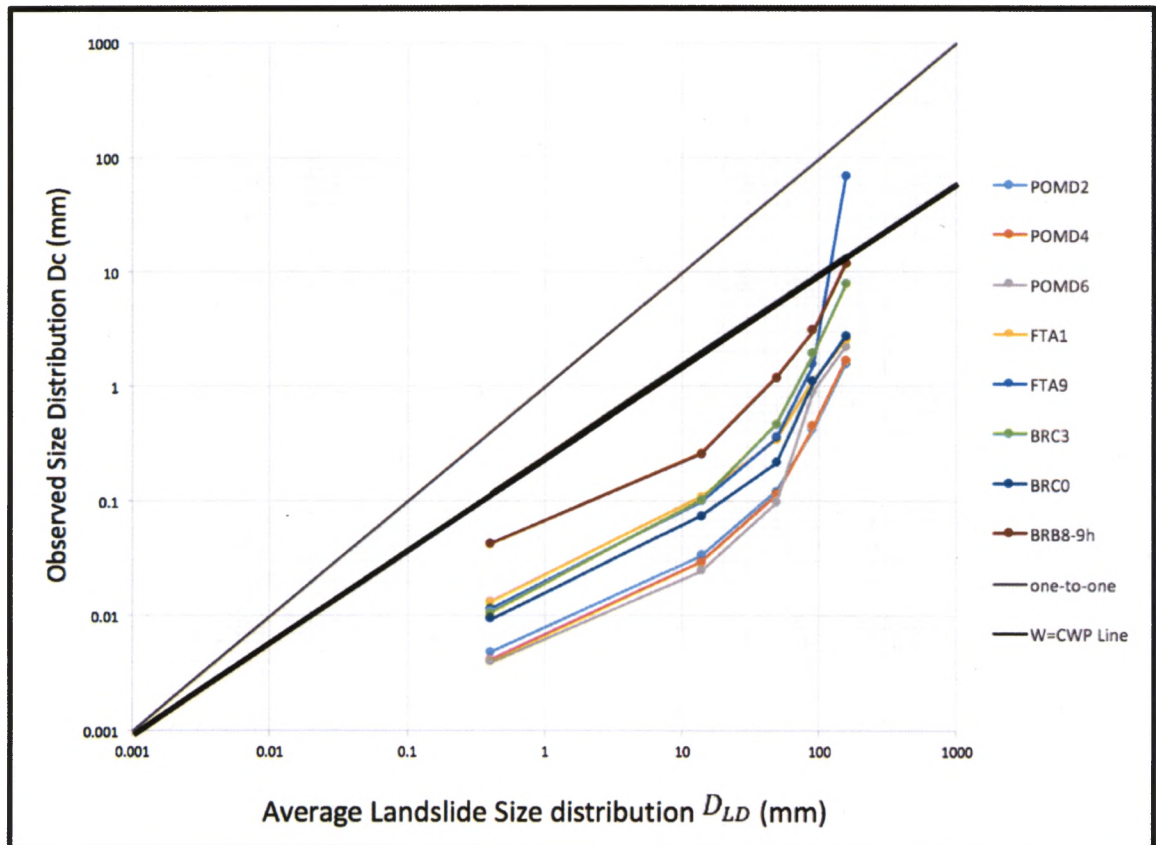


Figure 19. Feather River's first CWP model for particle size transformations across a range of chemical weathering potential, using Landslide point counts (D_{LD}) as the input. Light gray line represents the one-to-one line and the dark gray line represents the the average CWP for the sites. (**Notice** the order of CWP lines are flipped compared to Inyo creek. Distributions from higher elevations (POMD2, POMD4, POMD6) are now at the bottom of the CWP space. That is because the erosion rates are higher for the lower elevation sample, opposite of Inyo Creek, due to their location. Lower elevation samples are located in regions with higher slope gradients and thus are experiencing higher erosion rates).

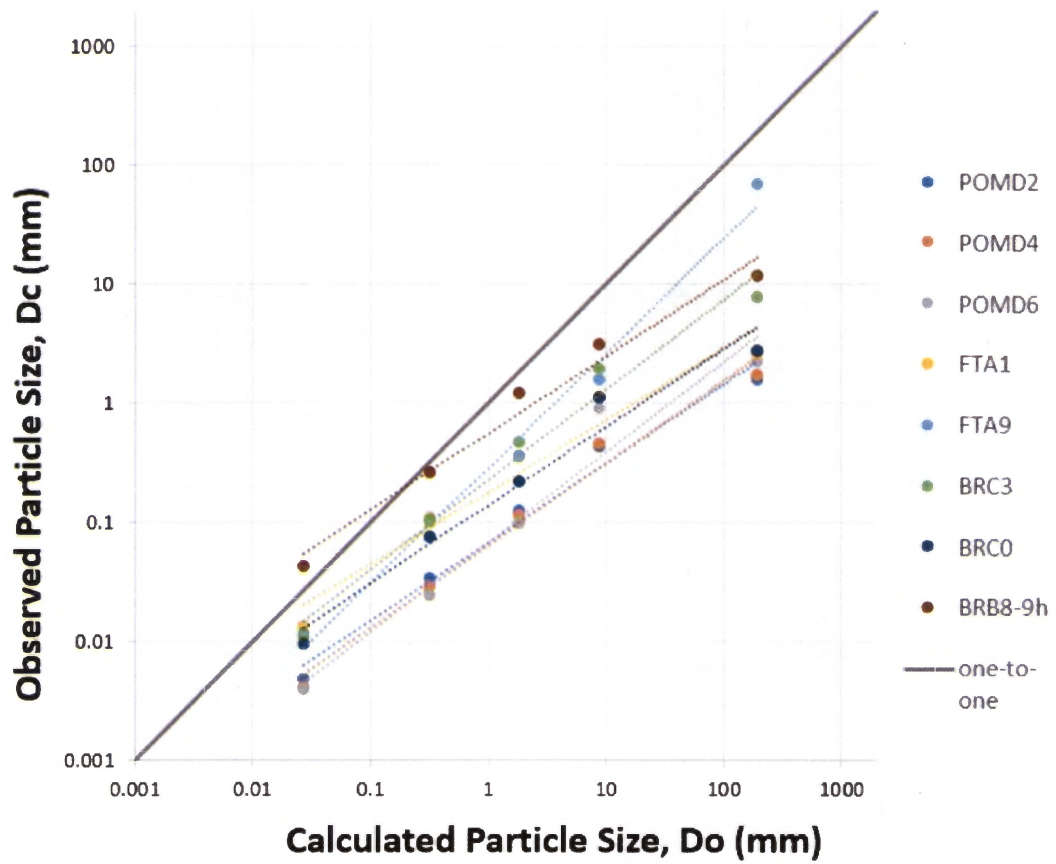


Figure 20. Individual sample sites plotted against CWP derived initial size distribution for Feather River. The distributions are fitted with power lines for cooperation to CWP lines.

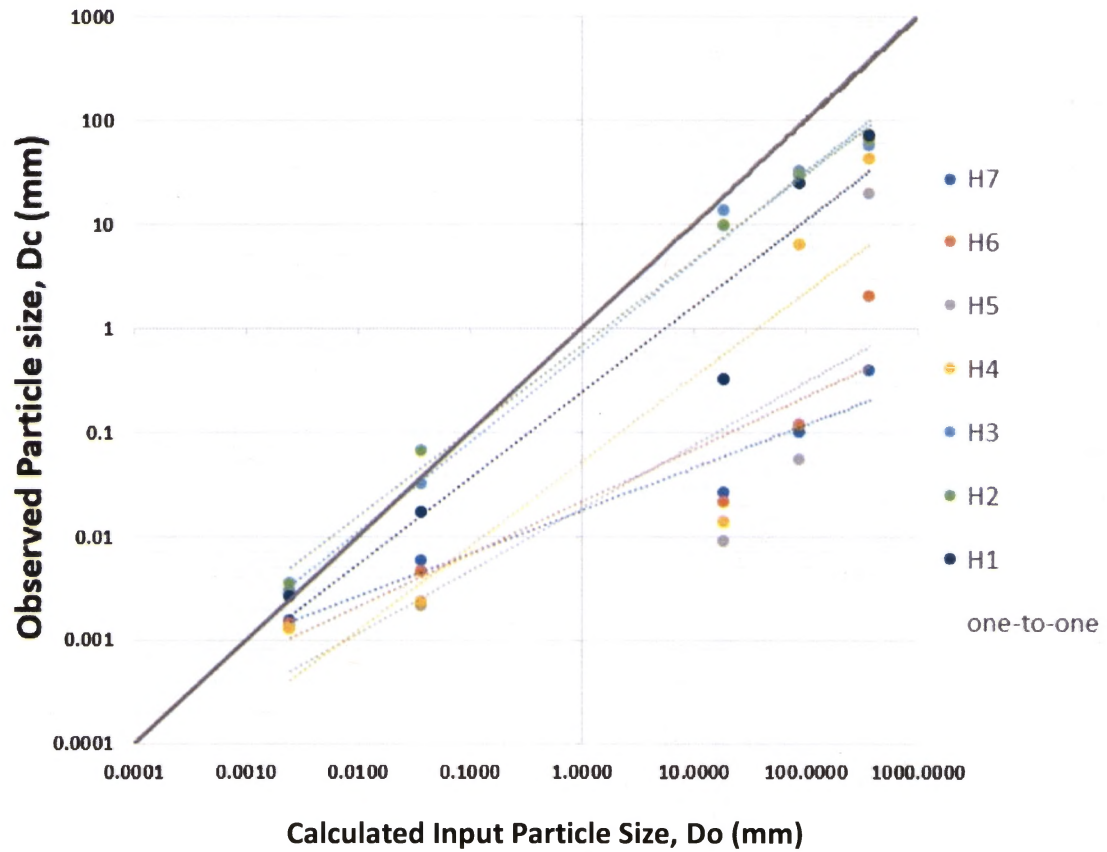


Figure 21. Individual sample sites plotted against CWP derived initial size distribution for Kohala Peninsula. The distributions are fitted with power lines for cooperation to CWP lines.

	Log(Aspect)	Log(Slope)	Log(Erosion)	Log(Weath)	Log(Precip)	Log(Temp)
Log(Aspect)	1.0000	0.0788	-0.4564	0.4677	-0.4379	0.4470
Log(Slope)	0.0788	1.0000	0.1398	-0.1329	0.1503	-0.1374
Log(Erosion)	-0.4564	0.1398	1.0000	-0.9993	0.9986	-0.9986
Log(Weath)	0.4677	-0.1329	-0.9993	1.0000	-0.9960	0.9975
Log(Precip)	-0.4379	0.1503	0.9986	-0.9960	1.0000	-0.9977
Log(Temp)	0.4470	-0.1374	-0.9986	0.9975	-0.9977	1.0000

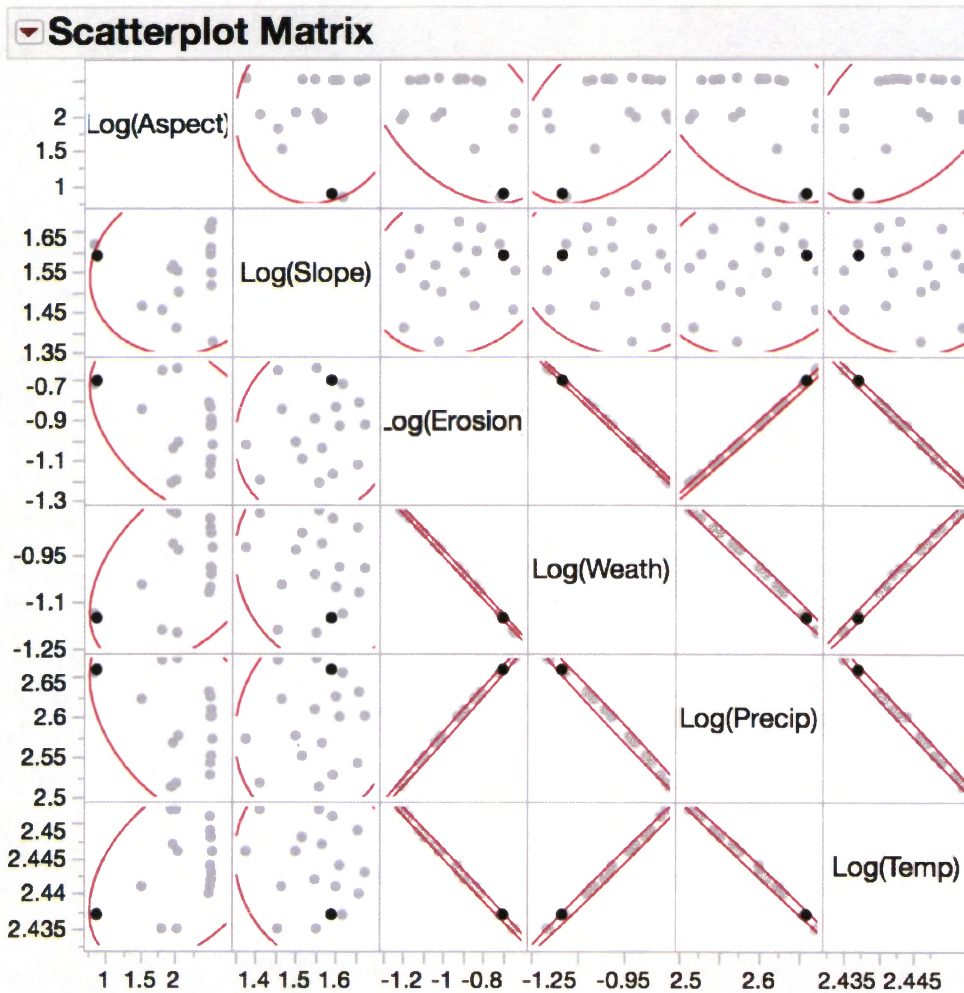
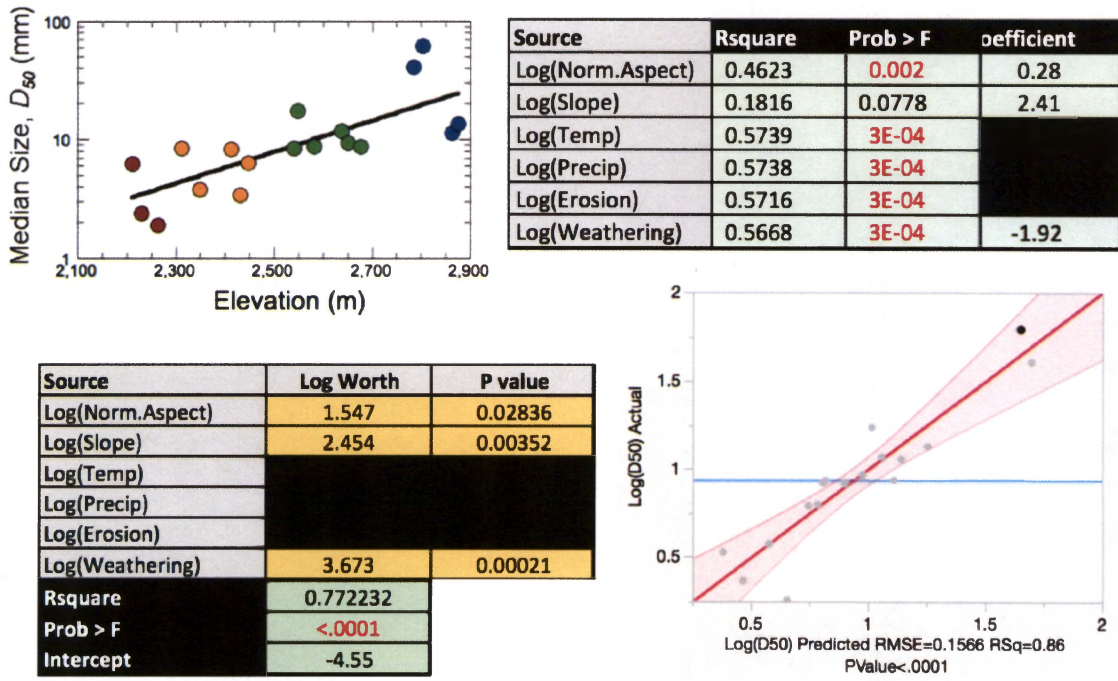
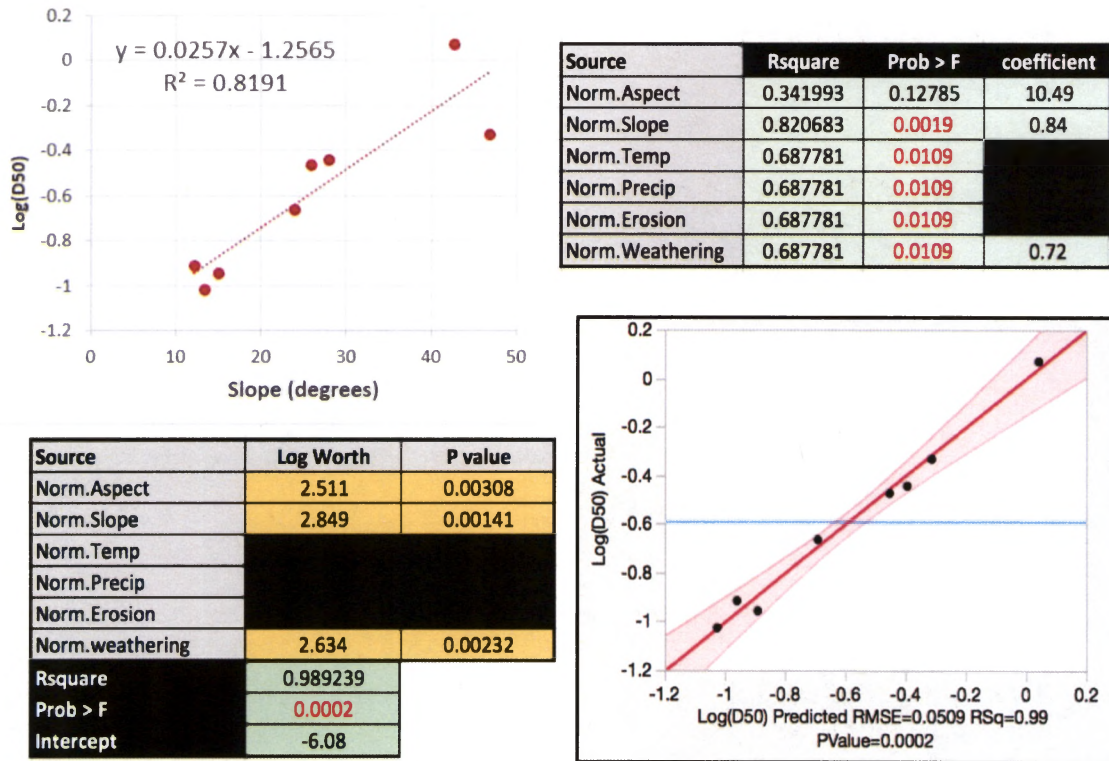


Figure 22. Pearson’s R multivariable correlation test ran on all 6 attributes. Temperature, precipitation, and erosion rate are all component of weathering equation (3).



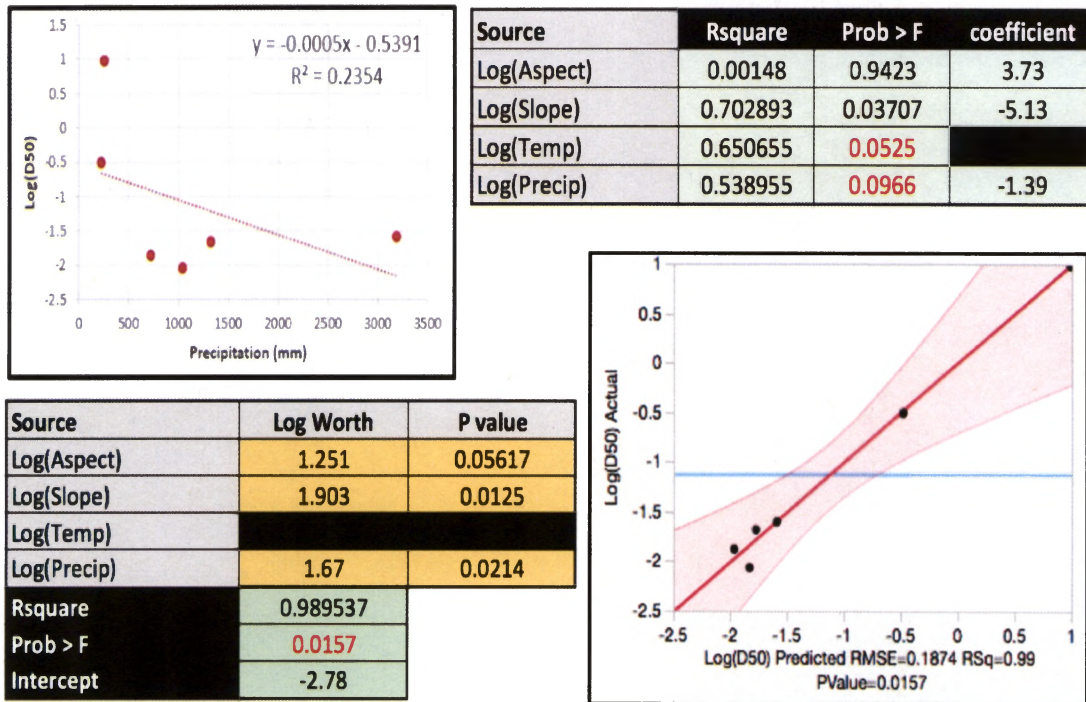
$$D_{50} = 0.00003 \text{ Weathering}^{-1.92} * \text{Slope}^{2.41} * \text{Aspect}^{0.28}$$

Figure 23. Inyo Creek’s D₅₀ plotted against elevation, shown as a possible control on D₅₀ (top left). D₅₀ varies significantly with many climatic and topographic variables. (top right). Multiple regression model explains D50 variation in terms of weathering function, hillslope gradient, and aspect (bottom table and plot).



$$\text{Log}_{10}(D_{50}) = -6.08 + 10.49 \text{ Aspect} + 0.84 \text{ Slope} + 0.72 \text{ Weathering}$$

Figure 24. Feather River's D_{50} plot against slope, shown as a possible control on D_{50} (top left). D_{50} varies significantly with many climatic and topographic variables. (top right). Multiple regression model explains D_{50} variation in terms of weathering function, hillslope gradient, and aspect (bottom table and plot).



$$D_{50} = 0.0017 * Precipitation^{-1.39} * Slope^{-5.13} * Aspect^{3.73}$$

Figure 25. Kohala Peninsula's D_{50} plot against precipitation, shown as a possible control on D_{50} (top left). D_{50} varies significantly with many climatic and topographic variables. (top right). Multiple regression model explains D_{50} variation in terms of precipitation, hillslope gradient, and aspect (bottom table and plot).

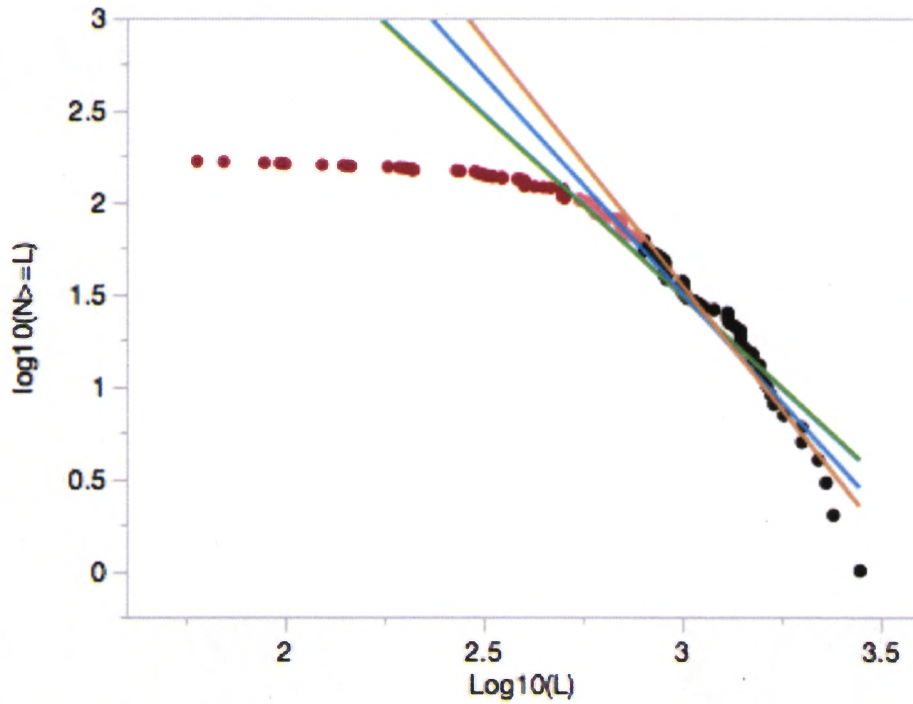


Figure 26. Plot of Bedrock Fracture Spacing from Inyo Creek, applied in the fractal model. The distributions do not follow a linear power relationship. The red points are all the smaller fracture lengths that were excluded to make a better fit. Fit line for the entire data set is (green). Fit line for half of the small length excluded is (blue). Fit line for all of the point counts excluded that were smaller than 2.75 cm (orange).

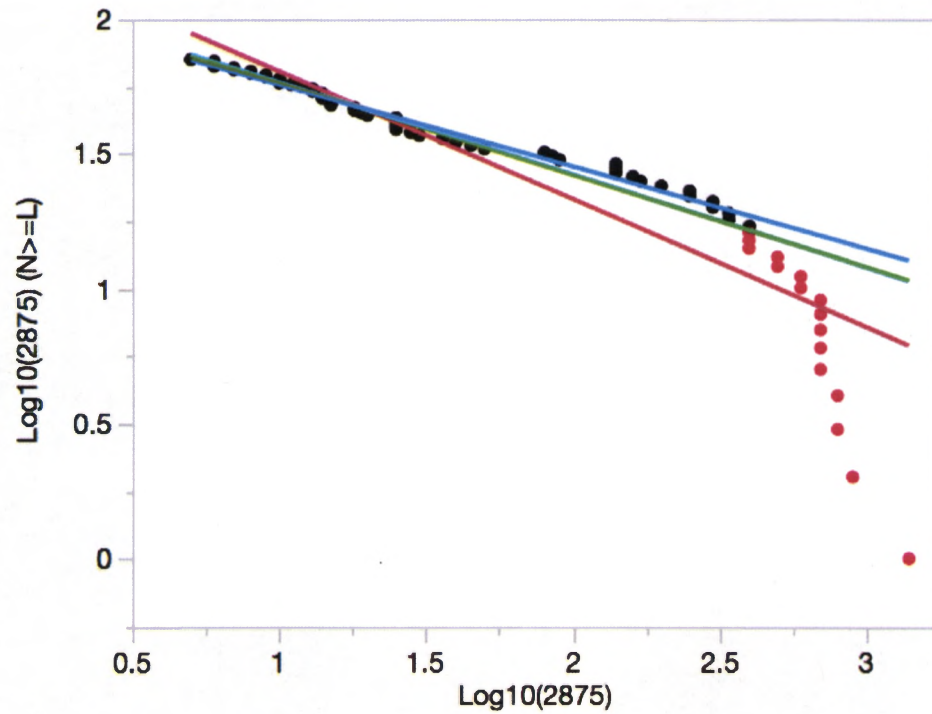


Figure 27. Plot of P2875 point counts from Inyo Creek's data set applied in the fractal model. The distributions do not follow a linear power relationship. The red points are large particle sizes that were excluded to make a better fit. Fit line for the entire data set is (red). Fit line for half of the large sizes excluded is (green). Fit line for all of the point counts excluded that were larger than 2.6 cm (blue).

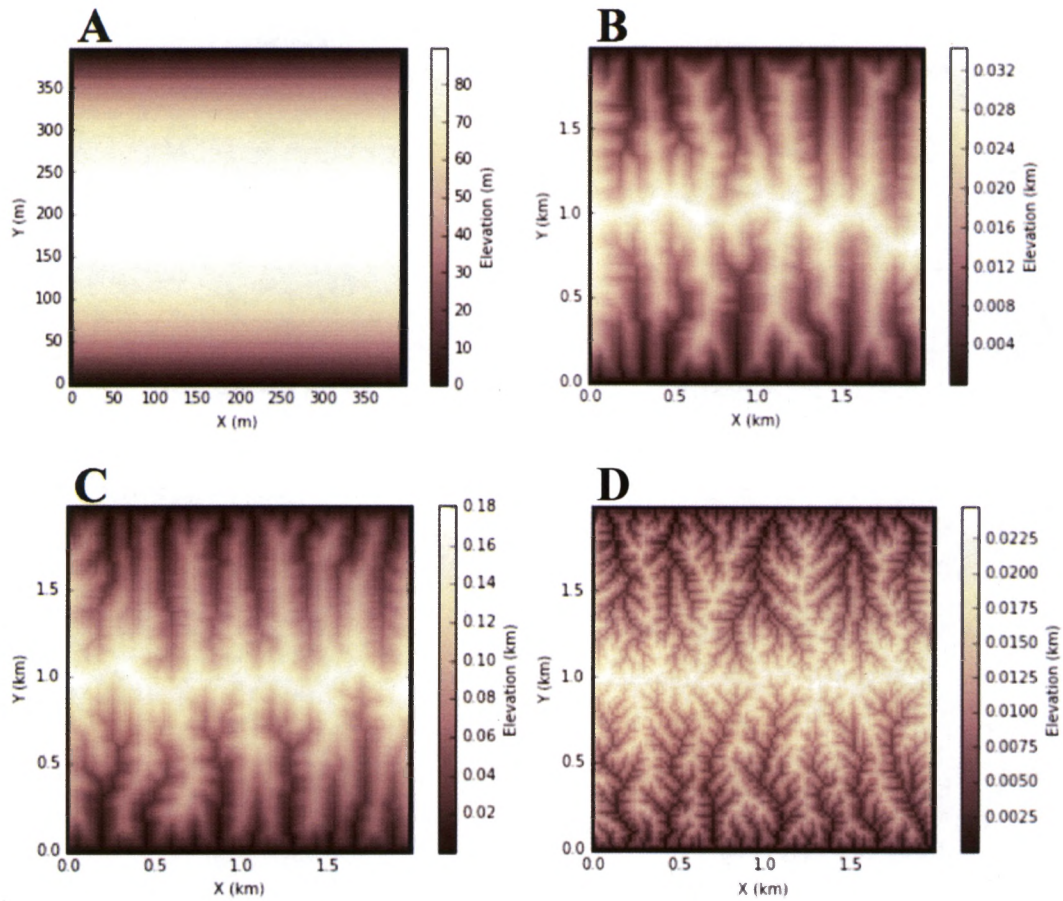


Figure 28. Typical output of the forward landscape evolution model simulation using LandLab. Combining three-component driver implementing linear diffusion, flow routing, and stream power incision. Landscape evolution from A to D, in 180 loops (each representing 1000 years).